UNIVERSITY OF COPENHAGEN
FACULTY OF SCIENCE

Master's Thesis

Master of Science on Climate Change

Marine heatwaves analysis thru climate models based on the CMIP5 program and observational data

José David Calderón Peña

Supervisor: **Jens Hesselbjerg Christensen** (KU,Copenhagen)

April 5, 2021

Abstract

Sea Surface Temperature representation over the worlds oceans varies across models. Climate models built in functions over-estimate the representations of Sea Surface Temperatures (SST's) in some regions and do the opposite in other ones. This builds up uncertainty around models skills to effectively represent climate modes and the ability to assess climate phenomena like Marine Heatwaves (MHW's). The present study compares 8 different climate models performance of SST's throughout a time-series that spans 150 years and compares it to an observational data set with a time-series spanning of 156 years to assess the appearance of MHW's. The analysis is done over 9 different regions across the globe with particular focus on the El Niño Southern Oscillation region due to its influence as a climate mode to the rest of the ocean regions. SST's threshold values from both climate models and observational dataset were estimated to create a ratio comparison between them. The findings of our study show that historical MHW's appearance from 1850 to 2005 are mostly seen at the Northern Hemisphere. SST's values from CSIRO-MK3-6-0 showed similar representation of threshold values compared to HadISST models at ENSO, Sub Polar Gyre, Tasman Sea and South of Alaska region. Sea of Japan region was overestimated by all models, being MPI-ESM-P and MPI-ESM-LR models who had the greatest values over HadISST thresholds overestimating by 1.8 and 2.0 times respectively. Continuous warming over months is seen in the Pacific Ocean, specially at ENSO region, where most models are able to represent ENSO phenomenon but do not show extensive warming around coastal areas as shown by HadISST. Most models agree with warming over most regions of the world on recent decades but time-series length of models does not capture last ten years of warming compared to HadISST dataset where most warming is appreciated near 2020. CMIP5 models resolution is useful to study MHW's distribution at large study areas. For a more detailed description of MHW's distribution and possible impacts on marine ecosystems, the use of finer resolution models to historical representation of MHW's and model projections in combination with Representative Carbon Pathway scenario (RCP) are recommended to avoid misleading adaptation measures.

Contents

List of Figures

List of Tables

1 Introduction

The increasing number, frequency and intensity of marine heatwaves (MHW's) has lighted the interest and concern on how to define a marine heatwave, how do they create, what is the current knowledge about MHW's and more importantly what are the implications of their observed increase to human activities, marine processes and biodiversity for present times and the years to come [Frölicher, T. 2018]. SST records are used to study MHW's formation. It is estimated that annual MHW's days have increased up to 50% from 1926 to 2016 and around 20% increased intensity since 1982 [Oliver ECJ. 2019]. Regional changes can export warming temperatures thru a range of teleconnection processes. Thus increasing the likelihood of the appearance of marine heatwaves. Sometimes this being linked thru teleconnection processes such as Rossby waves or climate modes like the North Atlantic Oscillation (NAO) or El Niño Southern Oscillation (ENSO) which have a major impact on sea surface temperature (SST). The previously mentioned processes can favour their predictability in areas where this processes are known to have an influence on MHW's formation [Holbrook, Neil J. et al, 2020]. The more these processes are understood in terms of their input to SST the better predictability over sea SST can be estimated years ahead of its appearance and effects. It is estimated that strong meridional heat transport linked to the Atlantic Meridional Overturning Circulation (AMOC), has a strong influence in the upper ocean heat content (UOHC), the top 700m, which can yield predictable temperatures between 2 to 12 years ahead of time [Borchert, L.F 2018]. The NAO is the most outstanding source of atmospheric variability in the northern hemisphere, it is related to exert strong circulation influence both meridional (north to south) and zonal (east to west) between 45°N and 65°N. When the NAO experiences a positive phase a low circulation patter is experienced around the Mediterranean sea. Its estimated to have a great impact over the Scandinavian energy sector. Norway's topography and climate makes the country suitable for hydroelectric power generation. A prolonged positive phase of the NAO during 1980's and 1990's created an excess of energy produced, allowing Norway to sell energy contracts with Sweden. At the beginning of 1990's the NAO was still in a positive phase, however, by 1996 NAO switched to a strong negative phase, this caused the water reservoirs to reduce their energy production. Dropping to 65% in 1996 from having a 95% of their reservoirs capacity a year before [Beaugrand, G. (2015)].

Located at the Southern Pacific, El Niño Southern Oscillation is the most influential global-scale hydro-climatic variability source. Some species can relocate to warmer areas where temperature allows its reproduction, some other like corals, cannot adapt to such rapid temperature shifts like the one occurred in El Niño event of 1997-1998, where 16% of the worlds corals died. Looking ahead in time about climate modes appearance could bring potential benefits to fisheries and tourism. Tagged skipjack tuna fish displacements yield information about its zonal displacement, allowing fisheries to forecast this species position several months in advance [Beaugrand, G.2015]. Three main time-scale categories are of interest for this study, it is within its forcing duration where teleconnections can help us explain changes in temperature and possible effects. A chart described below exemplifies the corresponding forcing type to the expected time-scale at which occurs and its effects on biodiversity.

Climate Modes			
Timescale	**Duration**	**Forcing type**	**Biodiversity response**
Decadal	10-90 years	PDO, AMO	Changes in species dominance (e.g. herring/sardine fluctuations)
Year-to-year (annual)	1-9 years	ENSO, NAO, Madden-Julian Oscillation	Coral bleaching, fish stock collapse
Intraseasonal	Less than 3 months	Heatwaves	Massive mortality of interstidal species

Table 1: Biodiversity responses to different forcing types [Beaugrand, G.2015].

Temperature is an important factor to many processes occurring in the ocean but also within species realm. Temperature regulates bacteria's growth and reproduction, photosynthetic activity and species reproduction timing and sex determination. It also has a direct effect on oxygen transport, when a critical temperature threshold is exceeded anaerobiosis starts rapidly threatening species survival. After a prolonged temperature stress, negative interaction between species develop (e.g. parasitism, disease, predation) and an entire web of interdependent species burdens. Anthropogenic climate change is expected to lead marine species to respond in four different ways: (1) by adjusting their physiology, (2) by triggering adaptive evolution, (3) by altering time/space distribution. When the previous measures fail, (4) extinction occurs. Species vulnerability to climate change is delimited by the species adaptive capacity, sensitivity and exposure to climate change. Species living within a narrow range of temperature (*Stenotherm species*) like invertebrates, are highly sensitive to warming or cooling temperature changes. This can potentially disrupt their biological functions [Beaugrand, G.2015]. The advantages of tracking MHW's and potentially forecast its appearance can yield social, cultural and economic benefits. Skillful prediction in this area can be useful for policy makers, industry and the scientific community for a better management of the ocean resources. When studying MWH's on timescales spanning over decades and centuries it is needed to account for inter-annual modes and forcings characteristics of the regions of interest to understand its possible appearance and properties. Whereas tropical oceanography would involve equatorial current systems and wind forcing associated with kelvin waves, Rossby waves and inter-annual air-sea modes (El Niño Southern Oscillation), the subtropical and subpolar latitudes would experience the influence of large-scale gyres with meandering and eddying limiting their extension to Western limits [Griffies, S. 2004]. For this matter this study will acknowledge the influence of large-scale marine processes coupled by teleconnections and climate modes to have a broad picture of MHW's development throughout the last 150 years.
Its important to bear in mind the mechanisms behind the MHW's formation to un-

derstand what this could mean in the context of a changing climate. For example, a constant melting of the poles can potentially disrupt some of the previously mentioned physical drivers by changing sea-water density composition. Thus, creating a diverse new set of effects around the world. Physical drivers behind the creation of MHW's are a combination of air-sea exchanges, advection by currents, horizontal and vertical mixing and entertainment of water into the mixed layer [Oliver, E.C. et al 2021]. This study does not include the physical drivers of Marine Heatwaves formation, instead analyses SST's as an outcome off all previous drivers involved.

1.1 Current Knowledge on Marine Heatwaves

The Pacific Ocean experiences the influence of a well known climate mode called El Niño Southern Oscillation (ENSO), which largely controls the climatic variability of the tropical pacific and has far-reaching meteorological and climatological effects around the world with consequences for human health, socio-economic systems and biodiversity. ENSO phenomena occur every three to six years, though their occurrence varies among authors. Its occurrence is sometimes related to an eastward movement of the ascending branch of the walker cell to a zone located between New Guinea and the international date line. Though it is thought to be a precursor of EL Niño events it is not always the case that this eastward movement of the Walker cell triggering ENSO events [Beaugrand, G. (2015)]. Some climate modes are particular to a region of the worlds ocean, while others like the Madden-Julian Oscilation (MJO) have planetary scale dimensions. MJO is a major source of weather variability at the equator having its greater influence over the Indian Ocean and the western and central part of the tropical Pacific. Uncertainties around its initiation, development and impacts of the MJO remain to be discovered but it is believed that it can influence the formation of cyclones at the tropics as well as triggering the Asian-Australian Monsoon system and creation of extreme flooding events on the western coast of America [Beaugrand, G. (2015)].
Understanding ocean dynamics is key to better assess the likelihood of MHW's occurrence and filtering the previous from natural cycles within ocean processes to determine whether we are experiencing a new trend within MHW's domain or going thru a stage of a cycle. Unusually warm water conditions like 'The Blob' event in the pacific ocean contribute to appearance of higher than normal SST's that can be enhanced by the Pacific Decadal Oscillatory (PDO) pattern. Improvements on the study of their relation can guide us to determine the occurrence of MHW's in the North Pacific. A similar task must be done for the rest of the world oceans to better assess the occurrence of MHW's [Mantua, N. J., & Hare, S. 2002]. The occurrence of MHW's is known to happen in areas with large SST variability like the central and eastern equatorial Pacific Ocean. Changes in the mean of SST are also found to be an indicator of changes in the properties MHW's but seems rather unclear which of both, changes in the mean of SST or its variance, has a dominant effect on Marine Heatwaves formation, rather is dependant on the region of study and the regional characteristics of the area allowing for a greater influence of them [Oliver ECJ. 2019]. MHWs formation is projected to increase under climate change due to increasing warming of the oceans. The role of anthropogenic climate change sets the background for a disruption of MHWs frequency, intensity and duration. MHWs characteristics have been consistently growing together with anthropogenic

forcing allowing for natural variability to grow out of its expected range [Oliver ECJ et al. 2021]. Warming of the oceans has not been uniformly distributed but rather scattered had been regional 'hot spots' owing its presence to regional attributes like western boundary currents [Wu L. et al 2012], as well as, areas with minimum warming or even cooling trends.

1.2 Main Objective

This study looks into 8 different climate model datasets of sea surface temperature records spanning from 1850 to 2005 for the CMIP5 climate models plus an observational data set. The observational data-set spans from 1870 to 2020 and is retrieved from the MetOffice observational dataset (HadISST). Sea surface temperatures will be studied thru analysis of detrended anomalies over the 99^{th} percentile in a monthly and decadal time scale plots. As well as sea surface temperatures detrended anomalies graphs extending thru the entire time series with marked threshold boundaries stating 1^{st}, 5^{th}, 95^{th} and 99^{th} percentiles. All climate models will analyze the same 9 regions of the world oceans and compare their performance to the observed temperatures from HadISST thru a Model/Observation ratio. Then the possible causes to MHW's occurrence as well as possible implications to marine biodiversity will be addressed in the discussion section. A special focus on species migration will be discussed as an outcome of MHW's effects.

2 Data

2.1 Climate Models and Observational Data

Studying climate series requires analyzing past data records from different data sets to have a fair description of the sea surface temperatures. Its worth to note that data-sets represent temperatures depending on the models configuration, for example, resolution and ensemble member of the model. Due to these particular characteristics, some models can be more sensitive to represent changes in areas of the ocean where other models do not. The datasets used for this study are strongly marked by annual cycles, which mask over trends and decadal oscillations. In this study eight different climate models are used to study sea surface temperature from 1850 to 2005. The consulted climate models for this study were retrieved from the Copernicus Climate Change Service (C3S) thru the Climate Data Store (CDS) as part of the fifth phase of the Coupled Model Inter-comparison Project (CMIP5, 2008-2012) [Taylor et al., 2012] and one observational data set from the Met Office Headley Center [Rayner et al.(2003)].
The HadISST is a monthly SST reconstructed time-series from 1871 to 2020 that captures regional and large-scale variations in SST trends. The HadISST applies data reconstruction techniques based on Empirical Orthogonal functions (EOF's) to capture the most influential modes of SST variability on a 1° area in a best effort to force atmospheric models to represent recent climate. One of the EOF-based techniques used is the reduced space optimal interpolation (RSOI), which reconstructs global patterns of long-term change as well as residual inter-annual variability patterns mixed with in situ SST measurements. In situ measurements of SST were collected from different sources, including bucket samples, fixed and drifting buoys,

voluntary observing ships using engine room intake water thermometers and to a lesser extent, sensors attached to the ships hull. Interpolation of SST where estimated when missing data for certain areas. Estimation of Sea Ice extent for the Antarctic region prior to satellite-based imagery (1973) was complemented by sea ice extension records from a sea ice extent monthly calendar covering the years from 1929 to 1939 published by *Deutsches Hydrographisches Institut* and from two Russian expeditions between 1947 and 1962. Improvements on satellite measurement techniques eventually helped covering larger areas of both hemispheres with more details, allowing for a better estimate of sea ice concentration. Challenges to precise estimation of sea ice extent are posed by thin layers of ice, which are not identified as such but as a mixture of open water and thicker layers of ice. As well as wet snow on top of ice disrupting microwave emission, thus confusing satellite readings. [Rayner et al.(2003)].

2.2 CMIP5 program

The present study observational data is retrieved from the fifth Climate Model Inter-Comparison Project (CMIP5). The overall goal of the CMIP is to provide Global Circulation Models (GCM) simulations to the scientific community that will allow the understanding of the climate's variability and climate change, the social implications of climate change impacts, further adaptation and vulnerability to climate change. It also provides valuable information to the Intergovernmental Panel on Climate Change (IPCC) reports. The fifth phase of Coupled Model Intercomparison Project (CMIP5, 2008-2012) was the product of a joint effort from 24 modelling centres running their models with prescribed conditions to produce a multi-model data set that would enhance our knowledge on the climate. The CMIP5 program strategy to study the worlds climate involves long term (century scale) and short term (10 to 30 years) modelling experiments using atmosphere-ocean global climate models known as AOGCMs. Some of the AOGCMs of the CMIP5 program account for biogeochemical components that include fluxes of carbon between ocean, atmosphere and land resembling the carbon cycles. These models are called earth system models (ESMs) and perform different simulations that are unique to this kind of models such as individual forcings or the influence of clouds and go deeper into those aspects. Short term models perform atmospheric chemistry and/or aerosols and regional air quality or predictions with 2010 Pinatubo like eruptions. The average spatial resolution of CMIP5 coupled models ranges from 0.5° to 4° for the atmosphere component and from 0.2° to 2° for the ocean component [Taylor et al., 2012]. The CSIRO-MK3-6-0 has a 1.875° x 1.875° resolution, both MPI-ESM-LR and MPI-ESM-P have a 1.875° x 1.875°, NorESM1-ME 2.5° x 1.89°, CanESM2 2.81° x 2.81°, IPSL-CM5A-LR 1.875° x 3.750° and INMCM4 1.5° x 2.5° longitude by latitude respectively [Mohan, S. et al 2019].

For the purpose of studying sea surface temperatures under equal characteristics for all models, their ensemble member initial conditions and covered period were chosen to be the same or as closest they could be between them. The following table shows 8 climate models and the observational data set:

Climate Models and Observational Dataset				
Dataset	**Variable(s)**	**Covered Period**	**Frequency**	**Ensemble member**
CSIRO-MK3-6-0, Australia	SST	1850-2005	monthly	r10i1p1
CanESM2, Canada	SST	1850-2005	monthly	r1i1p1
EC-Earth Consortium	SST	1850-2005	monthly	r10i1p1
IPSL -CM5A-LR, France	SST	1850-2005	monthly	r4i1p1
MPI -ESM -LR, Germany	SST	1850-2005	monthly	r3i1p1
MPI -ESM-P, Germany	SST	1850-2005	monthly	r1i1p1
NorESM1 -M, Norway	SST	1850-2005	monthly	r3i1p1
INMCM4, Russia	SST	1850-2005	monthly	r1i1p1
HadISST, MetOffice	SST	1870-2020	monthly	

Table 2: The table shows the climate models chosen for this study based on similar characteristics for a similar conditions assessment of SST's. All models are "historical experiment" category models.

MHWs are found at different locations around the world. Either influenced by teleconnection processes, dominant climate modes, human induced climate change or a combination of the previous. This study analyses the temperature records of 9 different regions of the world to have a broad picture of recent changes in sea surface temperature and MHWs occurrence.

Study Regions		
Region	**Latitude**	**Longitude**
Sub Polar Gyre (SPG)	50,61	320 - 351
El Niño Southern Oscillation (ENSO)	-10, 5	190 - 231
South Atlantic	-30, -15	330 - 359
Indian Ocean	-15, -5	70 - 90
Sea of Japan	39 - 46	150 - 170
East of Australia	-30,-20	160 - 180
Tasman Sea	-42,-36	155 - 165
East Coast of USA	40, 50	290 - 320
South of Alaska	40, 50	190 - 210

Table 3: The regions of study were selected after studying SST's above the 99th percentile in a monthly and decadal scale. As well as a map displaying the warmest regions above the 99th percentile without temporal division. The monthly, decadal and warmest region figures are shown at the results section.

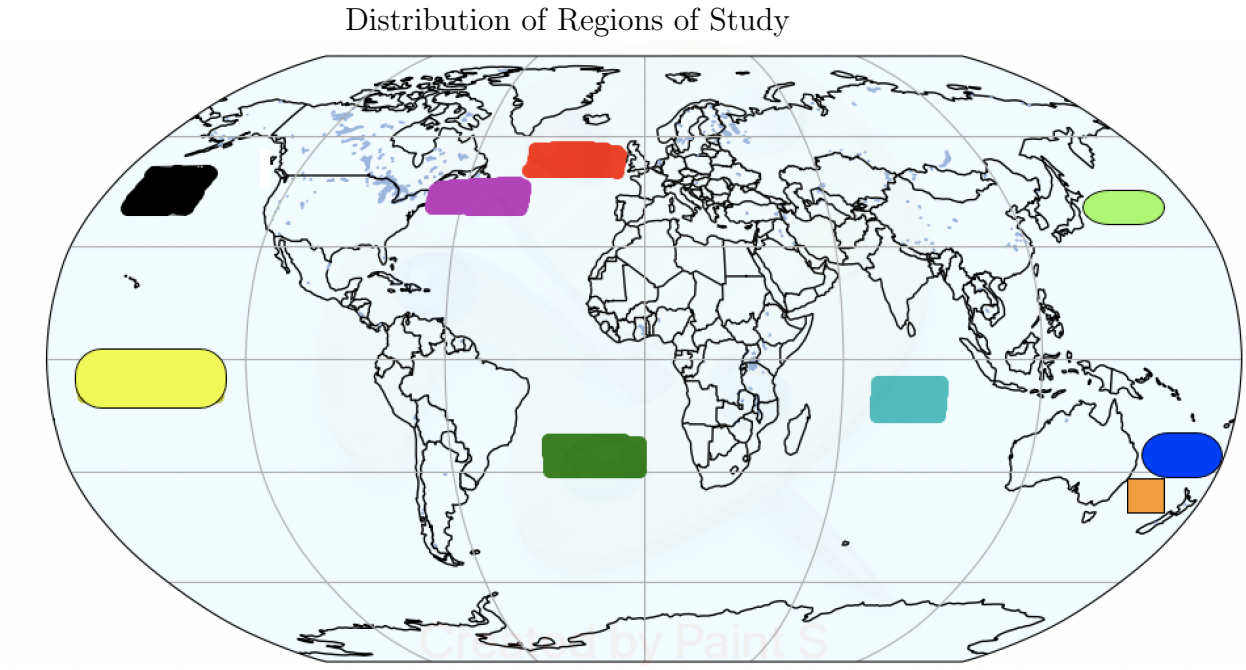

Figure 1: Considered regions for this study are shown at this figure. Areas of study were chosen based on observations SST's area of influence seen in Figures 3, 4 and 5 (shown at results section). South of Alaska (●), ENSO (●), East Coast of USA (●), Sub Polar Gyre (SPG) (●), South Atlantic Ocean (●), Indian Ocean (●), Sea of Japan (●), Eastern Australia (●) and Tasman Sea (●).

3 Methodology

Given the oceans heat capacity and dynamical scales, MHW's criteria must be carefully adapted to fit their characteristics into the purpose of the study. MHW's can happen in different scales and locations, such as small islands or along shore sections as well as regional areas, ocean basins and across oceans [Holbrook, N.J. et al 2020]. In general terms, MHWs are defined by their own characteristics (frequency, intensity, duration, spatial extent and severity) and the context at which MHW's are studied (temperature threshold, time and region of the world) [Collins, M. et al 2019]. In this study a MHW period will be considered when the temperature threshold above 99th percentile extends over 1 month. Spatial extent of MHW's will not be considered to their definition.

Some regions in this study have a known source of influence from climate modes that are possible to relate to the appearance of significant changes in the SST. The use of an observational data set helps compare which climate models are skilled enough to represent known ocean processes like ENSO.

3.1 SST Data processing

A record of sea surface temperatures (SST) spanning from 1850 to 2005 is used in this study for the CMIP5 models to have a broad picture of the fluctuating SST throughout the 1850-2005 period. For the MetOffice Observational Data Set the sea surface record is analyzed throughout its entire time-frame, meaning from 1870 to 2020. This helps to see where trends lead to and relate the trends to possible teleconnections and climate modes for marine heatwaves appearance given the location of the region studied. To evaluate the occurrence, frequency and intensity of MHW's in our cases of study, the sea surface temperature variable from the *CMIP5 of monthly data on single events* dataset was chosen. For this study the reference period will cover the entire time series, meaning 155 years, for the climate models and 150 years for the HadISST dataset. The chosen time span of the reference period makes it useful for studying physical climate characteristics with a focus on variability. The first step in the processing of our data will be to remove the seasonal cycle's to obtain the variability of temperature in our time series. Removing the seasonal cycles influence from our time-series will unveil the SST natural variation along our time-series. Seasonal cycles can hide long-term decadal oscillations, this is why it is important to remove the seasonal influence from our data-set. Followed by removing the seasonal cycles, an anomaly set will be constructed. The anomaly set is built by substracting the reference period monthly mean to the corresponding monthly mean value of our time series spanning from 1850 to 2005 for the CMIP5 models and from 1870 to 2020 for the HadISST dataset. Once the anomaly set has been constructed a detrending method is applied to make our temperature values oscillate around zero values. This gives us a clear point of view to evaluate the SST's [Wu et al., 2007]. Detrending allows an easier lecture of data values under and above threshold values. The threshold boundaries for our data will be defined by the 99^{th} percentile, 1^{st}, 5^{th}, 95^{th} percentiles were added as a reference to cooler temperature threshold boundaries.

The following figure shows the transformation of the data for the ENSO region from the HadISST dataset. All models used in this study follow the same steps illustrated in the following image. The image on top shows raw data with annual cycles, the removed influence of them is appreciated in the second image called "Anomalies". Finally, the third image shows detrended anomalies for the ENSO region of the observational dataset. The base period used for the climate models is different from the base period used in the observational data set. This is due to the length of the time series for models spanning from 1850's to 2005, whereas the observational data set spans from 1870's to 2020. Thus, the reference period that covers the entire time series, is as long as the time series for the climate model or the observational dataset.

ENSO Region from HadISST Dataset

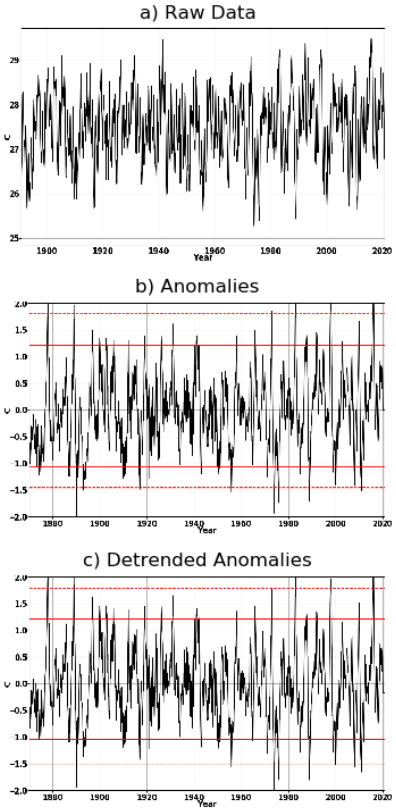

Figure 2: Transformation of data retrieved from HadISST is shown at this figure. The area corresponds to ENSO region. Plot a) Shows ENSO region's raw data. Plot b) shows the anomalies of ENSO using the years from 1870 to 2020 to form the base period. Plot c) shows Detrended anomalies across the entire time series. Only 95^{th} (—) and 99^{th} (- - -) percentiles values are used for the purpose of studying extreme warm temperatures. The values corresponding to the 95^{th} and 99^{th} percentiles for the ENSO region are 1.21 and 1.78 Centigrade above the reference period monthly average respectively. The 1^{st} and 5^{th} percentiles mark the extreme low temperatures with values of -1.52 and -1.04 Centigrade respectively.

A Model/Observation ratio chart was created to have a point of comparison between model results and HadISST results. This ratio comparison was built by dividing the percentile values (99^{th} dotted blue line and 95^{th} solid blue line) of every model and

region with its corresponding (99^{th} dotted red line and 95^{th} solid red line) percentile values from observations. As a result, the ratio chart built tells which model was closer to represent the observation values in every region.

4 Representation of Sea Surface Temperatures

4.1 Analysis of Sea Surface Temperatures

SST's were studied with different time-frame arrangements to plot MHWs in monthly and decadal scopes as well as a temperature profile where the highest temperatures over the 99^{th} percentile are found. HadISST dataset works with a 1° by 1° longitude and latitude resolution, hence, a more detailed distribution of sea surface temperatures compared to the models used in this study. Figure 3 shows consecutive SST's monthly temperature values over the 99^{th} percentile. This figure is created by using a mask over wrong values (for example, values over ice sheets or error values within the data set) and separates the temperatures values lasting less than one month. After applying the mask over wrong values, the temperatures under a defined threshold are ignored so only values over the threshold lasting more than a month will be considered to be plotted. The result then, is a filtered 99^{th} percentile values that remain over a month. The number of consecutive months over the threshold are counted and grouped by the number of months and plotted with a scale of color reflecting its duration. The results show in most of the plots a sustained duration of long lasting SST's in the equatorial Pacific, an area particularly known to be largely influenced by ENSO. The spreading of warm temperatures to higher and lower latitudes can be supported by teleconnections in both atmospheric and oceanic processes to other ocean basins. The North Atlantic Oscillation (NAO), an important climate mode in the Atlantic Ocean in addition to the Atlantic Meridional Overturning Circulation (AMOC) could potentially pave the way to marine heatwaves formation throughout the Atlantic Ocean. Rivers downstream produced by melting of ice sheets could help explain long lasting temperatures, which in cases like Greenland and the Antarctic coast show large areas with high temperatures lasting up to 10 months in a row in the observational data set in Figure 3. Besides the fact that extreme low temperatures are found at both locations (Arctic and Antarctic Oceans) and the increase on temperatures lasting over months does not necessarily reflects the appearance of MHW's in the nearby areas of the Arctic and Antarctic Ocean. The Indian Ocean experiences warm long-lasting temperatures that span up to 9 and 10 months in the observational data set as seen in Figure 3. Oceanic and atmospheric processes such as the Indian Ocean Dipole could cause warmer temperatures on either side of the Indian coast depending on its phase. The Indian Ocean Dipole and ENSO have a marked pattern and location. Sea surface temperatures are miss-represented in models CanESM2, CSIRO, NorESM, INMCM4, and IPSL around the Indian Subcontinent, compared to observations where a long lasting warm temperatures at this region can be seen in Figure 3. All models but INMCM4 seem able to represent ENSO to some degree, though its representation varies significantly among models. Being CanESM2 and MPI-ESM-LR models the ones that appear to represent ENSO and the surrounding areas influenced by ENSO in the Pacific Ocean in a more accurately way compared to HadISST dataset as seen in Figure 5.

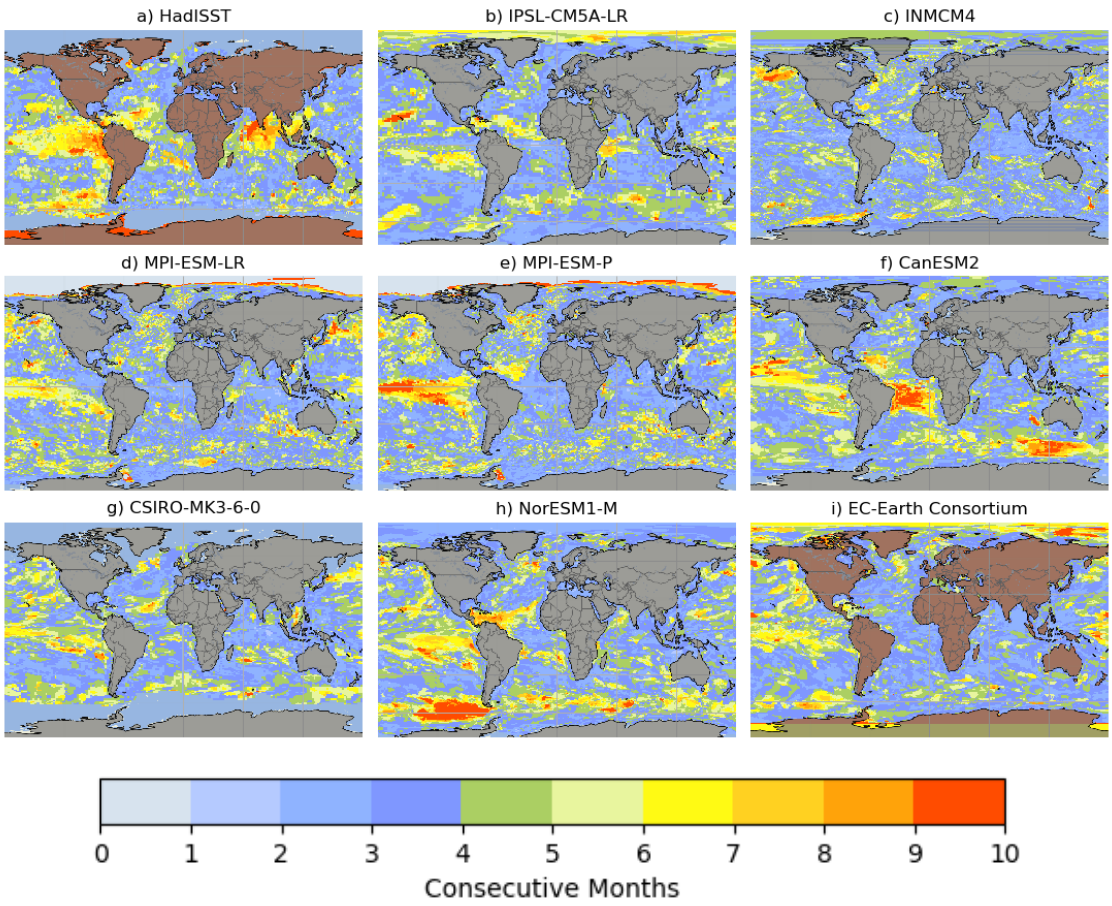

Figure 3: Time periods used comprehends from 1870 to 2020 (HadISST) and from 1880 to 2005 (Models). Light gray shading indicates the presence of sea ice at northern hemisphere, as shown at plots **d)** and **e)**.

Warming of the oceans happens at different regions and times due to a number of factors that include atmospheric and oceanic processes. Figure 4 divides the areas of the world's ocean warming by decades on which the highest warming was experienced thru a certain period of time. Most of the models agree on experiencing warming of the sea surface on larger areas around 1990's. It is common between models to show sea surface temperatures warming decades constrained to smaller areas at the beginning of the time series to then extend across entire ocean regions as the model approaches to recent decades. Recent warming decades appear closer to the poles as well, this is likely produced by melting of the ice sheets (particularly sea ice), but it is also worth to mention that a small increase of the extreme low temperatures experienced there could be miss interpreted as marine heatwaves in the areas near to the poles. Sea surface temperatures are also modulated by phase shifting of climate modes and the natural variability of the world's climate. Models **b)**, **f)**, **h)** and **i)** in Figure 3 show warming mostly occurring in the last 20 years, with warming happening all over the globe but most notably closer to the poles. Models **b)** in Figure 3 display warming extending thru large areas in the South Atlantic, extending from the coast of Brazil to a large fraction of the African continent Western coast.

The results of the HadISST dataset show a more defined warming areas by decade, where a 1990's warming decade around the Antarctic Ocean and another warming trend at the beginning of the 2010's at the North Atlantic is identifiable.

Most models display a variety of warming decades represented by different colors in very small areas that make it difficult to assess which was the dominant warming decade. Models **b)**, **c)**, **d)** and **g)** in Figure 4 show reduced areas of warming divided into several decades, which makes difficult to attribute warming to a particular decade besides the equatorial pacific, where warming its highly influenced by ENSO. Models **b)** and **f)** display a generalized warming towards the 1990's decade. Overall the leading warming decades appear around the 1960's in most models, whilst in HadISST dataset the leading warming decade is seen around 1990's. Models **h)** and **i)** show warming large areas of warming in early decades such as 1910's decade, being most noticeable in model **i)**.

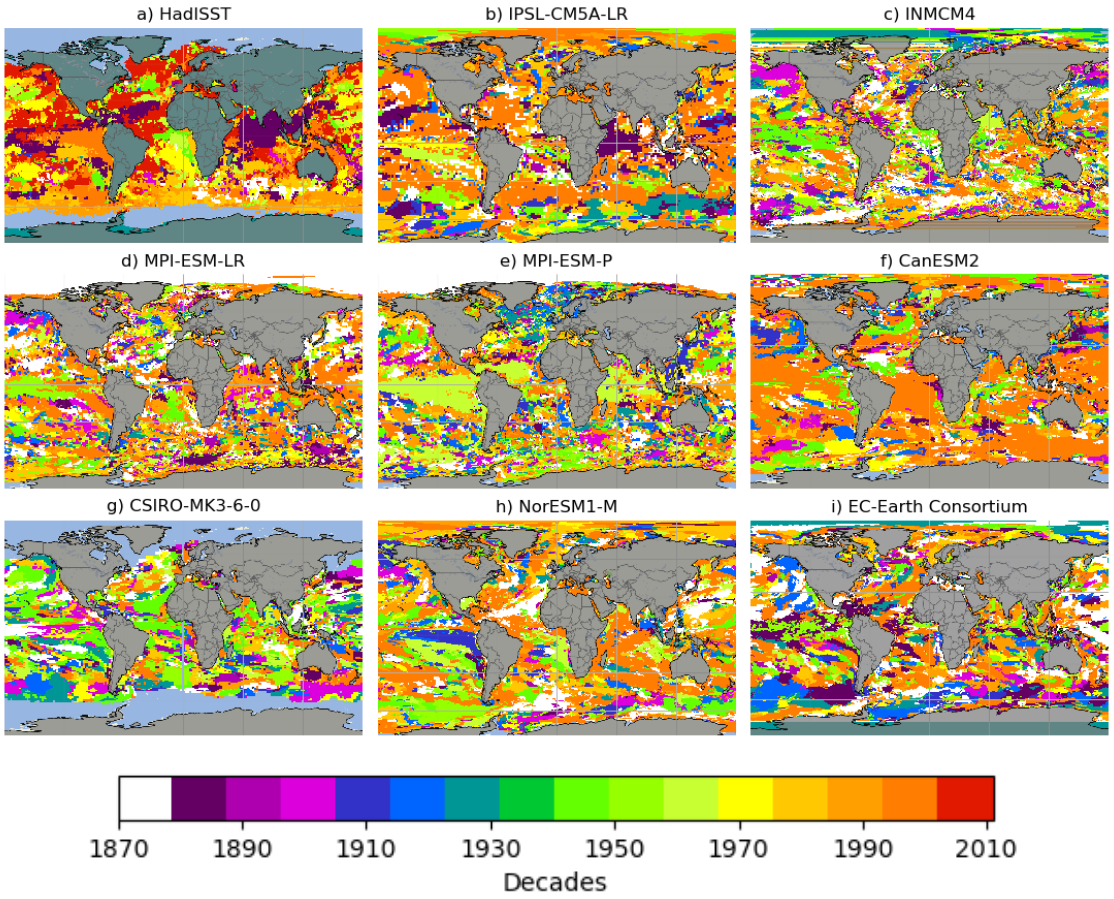

Figure 4: Shown at this figure are seen warming periods of time over the 99th percentile divided into decades for most extreme temperature values. Light blue shading indicate the presence of ice as seen over plots **a)** and **g)**. Time periods used comprehends from 1870 to 2020 (HadISST) and from 1880 to 2005 (Models).

Figure 5 displays the areas of the world that have experienced warming over the 99th percentile throughout the time-series. Again, representations for the warming temperature will vary between models but what it can be saved from this is that most of the models coincide with the HadISST dataset by showing warming at the ENSO region, with models **c)** and **i)** showing a weak ENSO. Warming is shown in most models around the North-Eastern coast of the United States of America and Canada and an area off the coast of Japan at which most models overestimate the temperatures shown by the HadISST dataset, with some models showing up to 2°

Centigrade above HadISST values. Though the HadISST dataset shows a much lower warming where most of the models over estimate the warming experienced in warming degrees and extension especially in the northern latitudes. The HadISST dataset shows a maximum warming of about 4° Centigrade around the Antarctic coast, which could be caused by melting sea ice. Models tend to overestimate not only the warming temperatures value but its extension, models **b)**, **c)**, **d)**, **e)** and **f)** in Figure 5 display warming reaching up to 5° across the Northern coast of Canada and Alaska as well as around Northern Europe extending all the way to Russia. It is likely that melting of sea ice off the coast of northern Europe and Russia is causing this warm anomaly to appear. At the southern Hemisphere, though warming of 1° to 2° Centigrade is experienced, shows a more stable warming at that settles mostly at 1° Centigrade, with some large areas reaching up to 2° Centigrade.

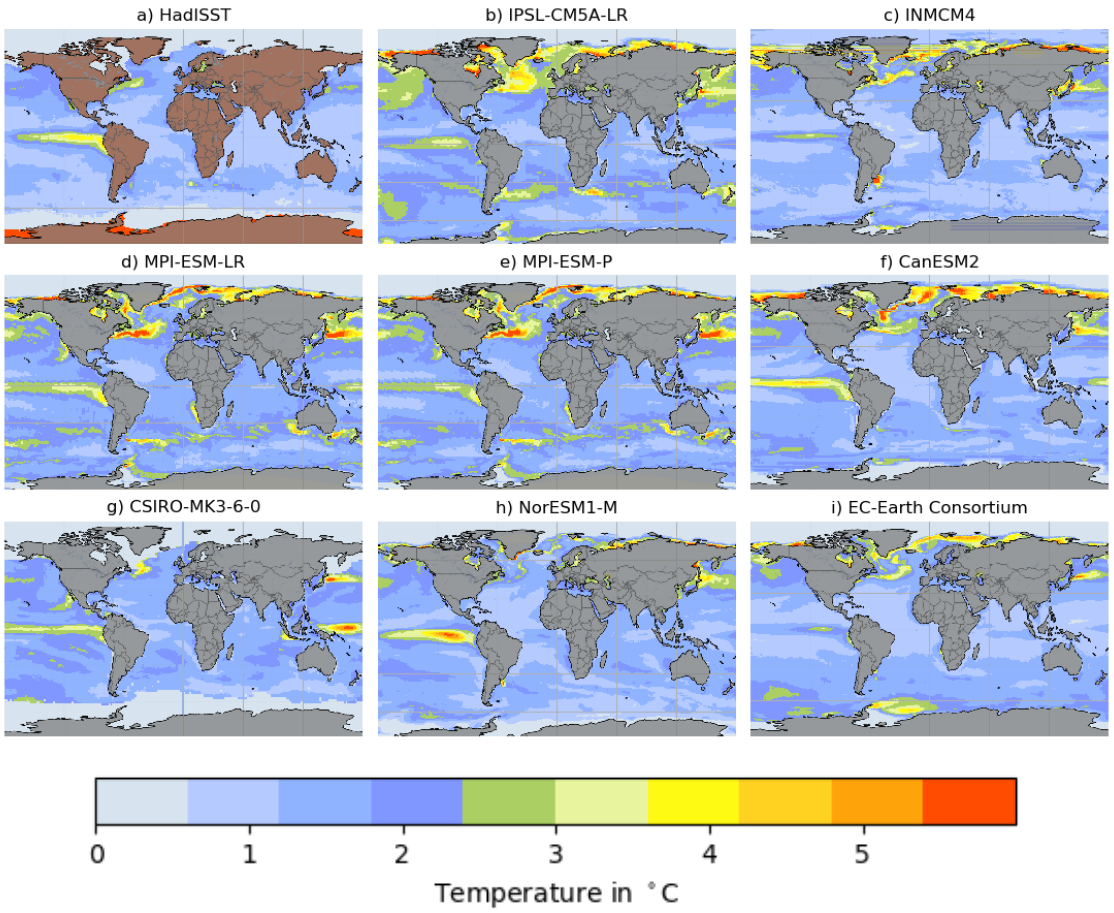

Figure 5: Shown at this figure are SST's values over the 99th percentile throughout the entire time series. Time periods used reaching from 1870 to 2020 (HadISST) and from 1880 to 2005 (Models). Areas in light blue shading indicate the presence of ice in North and South poles.

Qualitative description of Models and Observations

HadISST dataset representation of SST's are the point of comparison to models representation of the same variable. HadISST dataset sea surface temperature representation of sustained warming over the 99th percentile shows above thirteen areas with a 10 month in a row of constant warming mostly distributed Along the pacific Ocean and the Indian Ocean. Most of the areas are surrounded by degrading shades of color marking a seven months periods of time. The largest area is found at the ENSO region and the Caribbean sea as well as around the Indian Subcontinent. East and West coast of Greenland show two small regions of warming lasting up to ten months as seen in Figure 3. The dominant warming areas differ among decades, HadISST dataset shows five major warming decades mostly concentrated at the last 50 years of the time-series (1880, 1970, 1980, 1990, 2010) (Figure 4). 1880's warming decade is largely seen at the coastal areas of India and continuously extending to China. Smaller areas can be seen near Australia. A medium size area is found at the Caribbean sea and a smaller area at the South Atlantic. The Pacific Ocean shows scattered areas mostly at the Equatorial Pacific and South Pacific. 1970's decade is largely seen scattered throughout the Pacific Ocean, but it is in the South Atlantic where a large area extending from the coast of Brazil to the South Coast of Africa can be seen. Smaller sections can be seen in the Tasman Sea and off the Coast of Japan. 1990's decade is remarkably seen at the ENSO region and extending across the Southern hemisphere with smaller areas in the North Pacific close to Alaska. The rest of the oceans are covered by the 2010's decade which appear in large fractions of the Pacific and Atlantic Ocean and to a lesser extent in the Indian Ocean and South East Asia (Figure 4). HadISST dataset shows small areas of warming around the Coast of Japan where the Kuroshio current has some influence on SST's. Overall warming seen thru the observational data set seems limited to ENSO, East coast of United States and Sea of Japan (Figure 5).

CSIRO-MK3-6-0 model representation of SST's over the 99th percentile display three major areas at the Pacific Ocean lasting up to ten months, a considerable lower amount compared to HadISST. Continuous warming is appreciated in the North Atlantic region, over the Sub Polar Gyre area but in smaller areas compared to the ones found in the Pacific ocean. Consecutive months lasting up to ten months are also seen around Madagascar in the Indian Ocean and South Korea (Figure 3). The dominant warming areas found in CSIRO-MK3-6-0 show a warming around 1950's decade. Clearly seen across all ocean regions being most apparent at the North Pacific Ocean, ENSO region, North and South Atlantic, Western Australia and Indian Ocean. Decades 1890 and 1990 are also seen to be spread across large areas but with considerable less coverage than the 1950's decade. A weak representation of SST's suggests a shifting to La Niña event at the ENSO region (figure 4). Cooler temperatures cover most of the worlds map showing limited areas with warming to be seen in areas highly influenced by climate modes (Figure 5).

CanESM2 model shows four major areas with smaller areas lasting up to 10 months found at ENSO region, Caribbean Sea, South Atlantic Ocean and South of Australia (Figure 3). Greatest warming in the time-series is seen in decades 1910, 1950 and 1990. 1910's decade displays warming areas in South American coast, Indian Ocean

and North Atlantic Ocean. 1950's is seen in North and South America's coast as well as close to the Antarctic Ocean, south Africa's coast and East of Africa as well as North Atlantic, North West Greenland and North East Russia. 1990's leads the warming over a vast majority of the world oceans across all regions (Figure 4). The overall warming exceeding the 99^{th} percentiles is found at the North pole, extending from Alaska and Canada to Greenland. And all over the European coast to Russia in a combined temperature oscillating between 4° and 5° Centigrade.

Several regions across the Pacific Ocean reaching up to 10 consecutive months over the 99^{th} percentile can be see at **EC-Earth C.** model, ENSO region is dominated by areas of warming lasting up to seven consecutive months with little spots reaching up to ten months. Sustained warming is mostly seen across the Pacific Ocean with the Northern latitudes having the warmest regions. The Sub Polar Gyre (SPG) region shows warming reaching up to 10 months in a very small area, mostly surrounded by seven consecutive months of warming areas. The South Atlantic region, off the coast of South Africa displays scattered sustained warming reaching over five months. The largest and longest sustained warming region is appreciated over the North coast of Russia. The Antarctic region also displays sustained warming lasting up to seven and ten months mostly constrained to coastal areas (Figure 3). Areas with the largest warming decades are marked mostly by 1910's and 1990's decades with a large fraction of the ENSO region dominated by 1880's and 1950's decades. Being the 1990's decade most notable across all regions (Figure 4). Overall warming over the 99^{th} percentile is appreciated across the north pole, mostly north of Europe and around Alaska and a rather big area in the Antarctic coast (Figure 5).

IPSL-CM5A-LR model shows areas of sustained warming mostly at the Indian Ocean near the coast of Kenya. Further down into the Indian Ocean East of Australia, a hot spot reaching up to 10 months can be seen. One area clearly identifiable as lasting 10 consecutive months in the north pacific is seen off the coast of Mexico, being the largest and long lasting region shown by this model (Figure 3). The 1880's leading warming decade is seen over North and south Pacific Ocean. Besides a prominent area on the East Coast of Africa extending to the Indian Subcontinent, as well as an area Southeast of Australia. The 1930's decade manifests scattered close to the poles, whilst the 1990's decade covers the rest of the worlds ocean (Figure 4). A large area of the northern hemisphere presents warming of about 3° Centigrade in North Pacific and North Atlantic Oceans, with north coast of Alaska, Canada and Europe showing the highest warming temperatures, probably due to melting sea ice (Figure 5).

Model **MPI-ESM-LR** sustained warming over months display a large number of spots. Between twenty to thirty small areas where warming experiences long duration above seven months and around twenty nine spots reaching up to ten months of sustained warming The Pacific Ocean is the region that holds the most number of hot spots, being the Sea of Japan the most extended area of high warming. A long lasting area of warming around the North pole warming can be seen near the ice. The warm temperatures registered by this models could be biased by melting sea ice (Figure 3). Warming is mostly experienced over 1940, 1980 and 1990 decades. 1940's decade has medium to small scattered warming areas in the pacific coast at

the ENSO region and down south close to the Antarctic coast as well as in the West coast of Africa and the North Atlantic Ocean and all the way up to the Northeast coast of Greenland. Smaller areas of the 1940's decade can be seen in South East Asia and around The Australian Continent as well as close to the Coast of Japan and the China Sea. Overall, 1990's decade covers most of the oceans. But smaller fraction of warming from other decades are well distributed, specially in the Southern hemisphere. Overall warming over the 99^{th} percentile is seen over coastal areas of Northern Canada, South of Greenland and North of Europe, probably caused by melting of sea ice. A warm current extending off the East coast of the United States and the Sea of Japan can be seen in Figure 5. ENSO region is well appreciated extending from the coast of Peru into the Pacific Ocean with an average temperature of 3° Centigrade. South of East and Western Australia display high levels of warming in reduced areas (Figure 5).

Sustained warming over 99^{th} percentile in Model **MPI-ESM-P** is seen mostly over ENSO region. Smaller areas are found at the South of Argentina's coast, North of Russia and East coast of Africa, Southwest Australia and South of Japan's coast. A long area of the Arctic experiences long lasting warming temperatures over consecutive months reaching up to 10 consecutive months (Figure 3). The leading warming decades are 1910, 1960 and 1990. 1910-1920's decade is scattered across multiple regions being at the China's coast where it has its larger distribution. The 1960's decade its notably the most extended warming decade, having its presence in the ENSO region, Caribbean Sea, North and South Atlantic ocean, East coast of Africa and extending thru the Indian Ocean to the coast of Myanmar. Ultimately the 1990's decade appears scattered around the globe having a stronger presence in the south east Asian region but also seen in the North pacific region (Figure 4). A similar distribution of the overall warming to MPI-ESM-LR is seen across the Northern hemisphere. ENSO region shows cooler temperatures and also a narrower distribution of ENSO. The Antarctic coast show a small area of Warming that reaches up to 4° Centigrade near the coast of Argentina and a similar warming distribution around southern Australia but now in an semi-continuous warming layer that extends from Southwestern Australia to the coast of Argentina (Figure 5).

Model **NorESM1-M** shows five important areas with warming up to ten months, being four of them in the Pacific Ocean. High levels of warming are seen across the Pacific Ocean most notably at ENSO region and North Pacific coast of Mexico and United States. A small area near the Sub Polar Gyre region shows a long lasting area of warming as well as surrounding areas in smaller sections. Long lasting temperatures across the Antarctic ocean are seen, lasting on average seven months but reaching up to ten months in small sections. The Southeast coast of Russia and coast of Japan also experience long lasting temperatures reaching up to six months on average. The biggest area is shown near the Antarctic Coast close to the South Coast of Chile (Figure 3). Decades with greatest extension are 1910, 1940 and 1990. 1990's warming decade is clearly seen at the ENSO region but also scattered around the south Atlantic near the Coast of Africa and to a lesser extent in the Indian Ocean. The 1940's decade is mostly represented at the equatorial and south pacific ocean but with little areas in the North Pacific as well. The rest of its appearance is mostly constrained to the Southern hemisphere along the Antarctic coast. Smaller

areas can also be seen in the China Sea and near the coast of Japan (Figure 4). Overall warming is seen mostly at coastal areas of the northern hemisphere. East coast of Alaska, Southeast of Greenland, North coast of Russia holds the highest warming portrayed by this model reaching up to 5° Centigrade. The coast of Japan also displays warming reaching up to 4° Centigrade. El Niño phenomenon reaches a high warming over 5° Centigrade and it is represented with a smaller extension compared to observations.

INMCM4 model results of SST's analysis displays five small regions located in the southern hemisphere showing warming areas that last up to ten months, these regions are found near the Antarctic coast. The Northern hemisphere also shows warming areas around the coast of Alaska, East coast of Canada and northern Russia with an average of 6 months of duration. The Atlantic ocean displays scattered areas of sustained warming along its extension, with most areas of sustained warming near the East coast of the United States. Smaller regions of sustained warming are seen between South Africa's coast and Western Australia lasting up to 5 months (Figure 3). The greatest warming is mostly seen in decades 1890 and 1940. 1890's warming decade is found around the coast of Alaska and western Canadian coast as well as scattered in smaller areas throughout the pacific ocean having a rather medium size area near the Antarctic coast. The Atlantic Ocean also presents small areas across its extension but having slightly more areas in the South Atlantic. The 1940's decade is seen around ENSO region and at the Southern Pacific, close to the Antarctic Coast. But also in coastal areas around the African continent, Australia, South East Asia and East Coast of Japan. The 1940's warming decade is prominent across the entire Northern Hemisphere, mostly over Canada and Greenland (Figure 4). Besides a high warming temperature reaching up to 6° at the Coast of Argentina, the highest warming is shown at the Northern hemisphere especially at the North coast of Russia, Europe around Greenland and Alaska. A warm temperature reaching up to 4 ° stems from the East coast of Canada towards Europe (Figure 5).

4.2 Climatologies and Models Ratio

SST's anomalies with a 95^{th} and 99^{th} percentile threshold were created to work with the most extreme temperatures, meaning looking into the 5% and 1% warmest temperatures throughout the entire climatology. The 99^{th} percentile filters the warmest values among all temperatures. This gives us a better perspective of MHWs assessment. The chosen regions correspond to areas where the effect of climate modes and/or important ocean processes occur (ENSO, AMOC, NAO) and could lead to the creation or disruption of marine heatwaves. HadISST results are taken as a reference across models. The following charts show the ratio between models and observations across all regions. The ratios were obtained dividing the modelled value by the corresponding observations values.

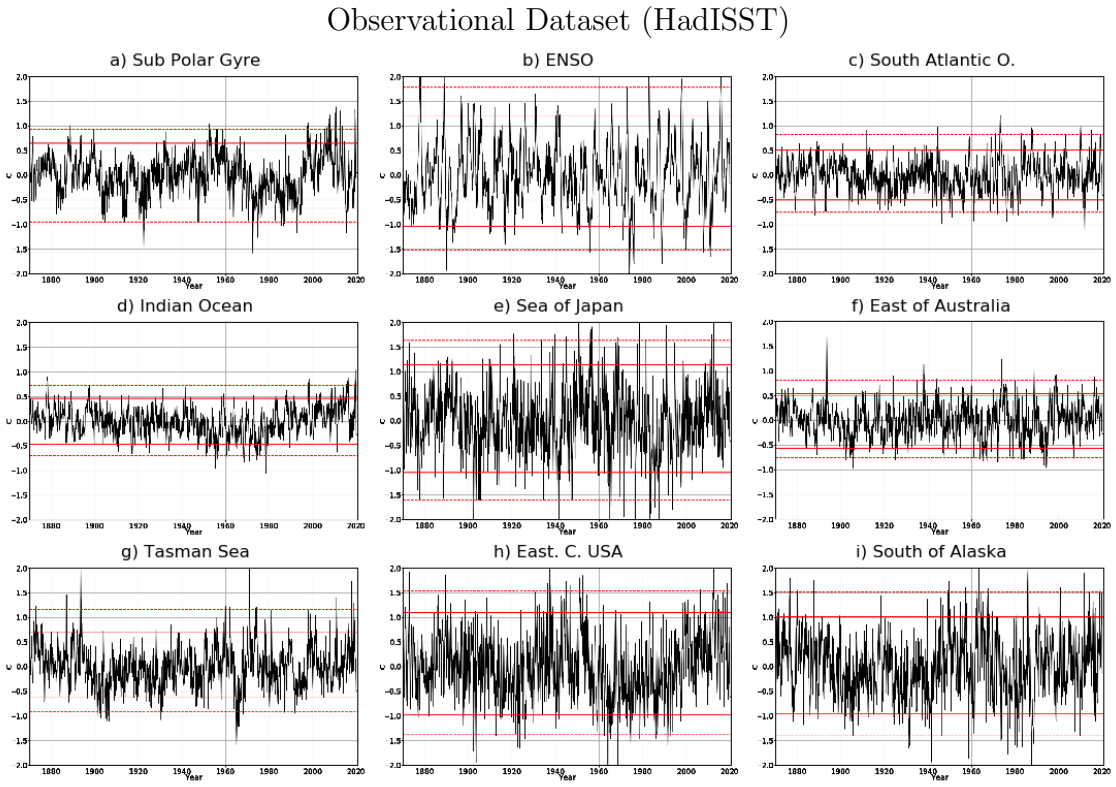

Figure 6: Plots displaying the 99th and 1st percentiles are marked a red dashed line (- - -), whilst 95th and 5th percentiles are marked by a solid red line (—).

The 99th and 95th percentiles were computed over the 9 different regions to obtain the temperature threshold and their equivalent to Centigrade were taken to elaborate the ratio charts. These values from models were used to obtain the ratios as every models own 99th and 95th percentiles value were estimated.

Observational Data-Set									
Percentile	**SPG**	**ENSO**	**South Atlantic**	**Indian Ocean**	**Sea of Japan**	**Eastern Australia**	**Tasman Sea**	**East Coast USA**	**South of Alaska**
95th percentile	0.64	1.21	0.50	0.46	1.14	0.54	0.70	1.09	1.01
99th percentile	0.9	1.78	0.82	0.72	1.63	0.81	1.16	1.53	1.51

Table 4: The chart displays the computed 95th and 99th percentiles for every region. Values inside the boxes correspond to Centigrade.

The following ratio charts are to give a perspective of which regions of the worlds are better estimated by models. A ratio under 1.0 would mean that the model underestimates the temperatures at the particular region. In the other hand, a value over 1.0 would mean that the model over estimates temperature. To make our reading of the ratio charts easier the values of 1.0 will be highlighted, meaning that the model at that region is able to represent the temperature values are similar to the HadISST dataset.

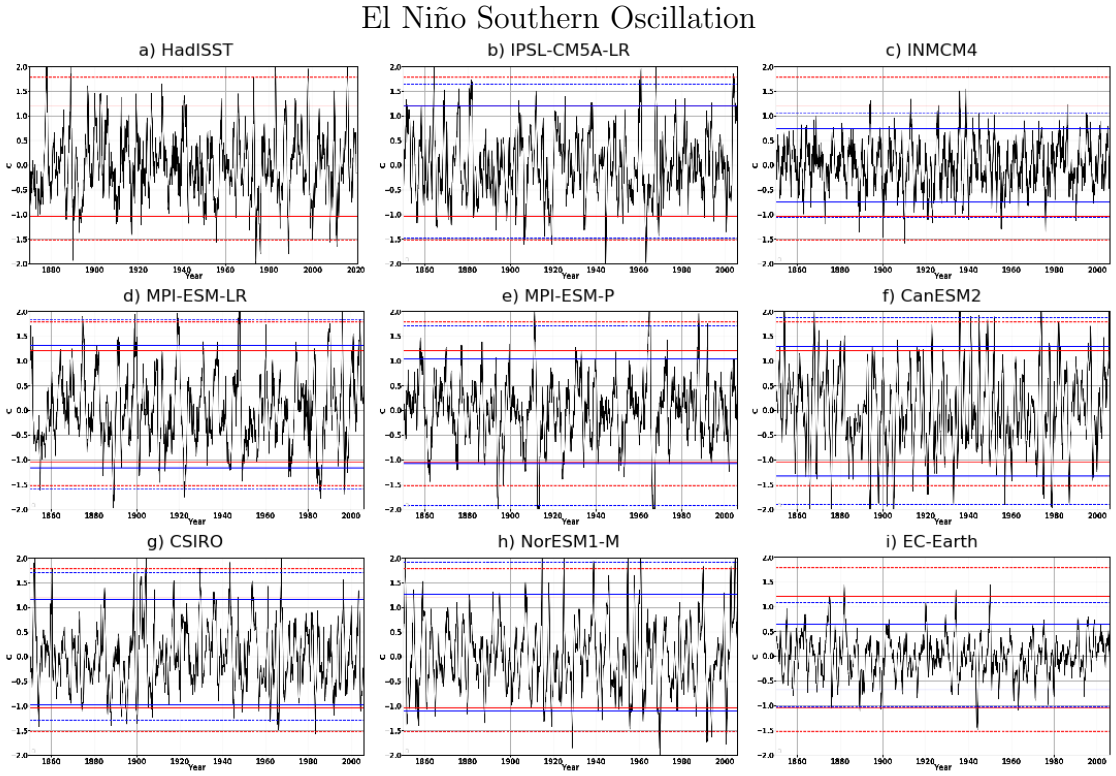

Figure 7: Red color lines represent the Observational data set 99th (- - -) percentile and 95th (——) percentile for ENSO region. The models 99th (- - -) and 95th (——) percentile for the ENSO region are represented by blue lines. HadISST dataset spans from 1870 to 2020 whilst the models spans from 1850 to 2005.

El Nino Southern Oscillation								
Percentile	**EC-Earth**	**MPI-ESM-P**	**MPI-ESM-LR**	**CanESM2**	**CSIRO-MK3-6-0**	**INMCM4**	**IPSL-CM5A-L**	**NorESM1-M**
95th percentile	0.64	1.03	1.3	0.71	1.16	0.73	1.12	1.26
99th percentile	1.08	1.7	1.83	0.95	1.7	1.06	1.64	1.92
95 ratio	0.53	0.85	1.07	0.59	0.96	0.60	0.93	1.04
99 ratio	0.6	1.0	1.0	0.5	1.0	0.6	0.9	1.1

Table 5: Chart showing 95th and 99th percentiles performed by models. Percentile results were rounded to one decimal point. Ratios (red boxes) were created by dividing models results by corresponding percentile from HadISST. Pink shading highlights a similar representation of models to HadISST dataset results.

Three out of the 8 models are able to precisely estimate the temperature threshold values at the ENSO region. CanESM2 model has the lowest ratio value, underestimating the temperatures at the ENSO region with a 0.5 value. Overall the ENSO region is an area at which most of the models are able to represent the threshold temperature values correctly whilst the rest of the models estimates get very close to their precise representation. The ENSO region finds itself in a geographical position where annual cycles are not present, therefore all models seem to do a "good work" on subtracting the annual cycle's influence.

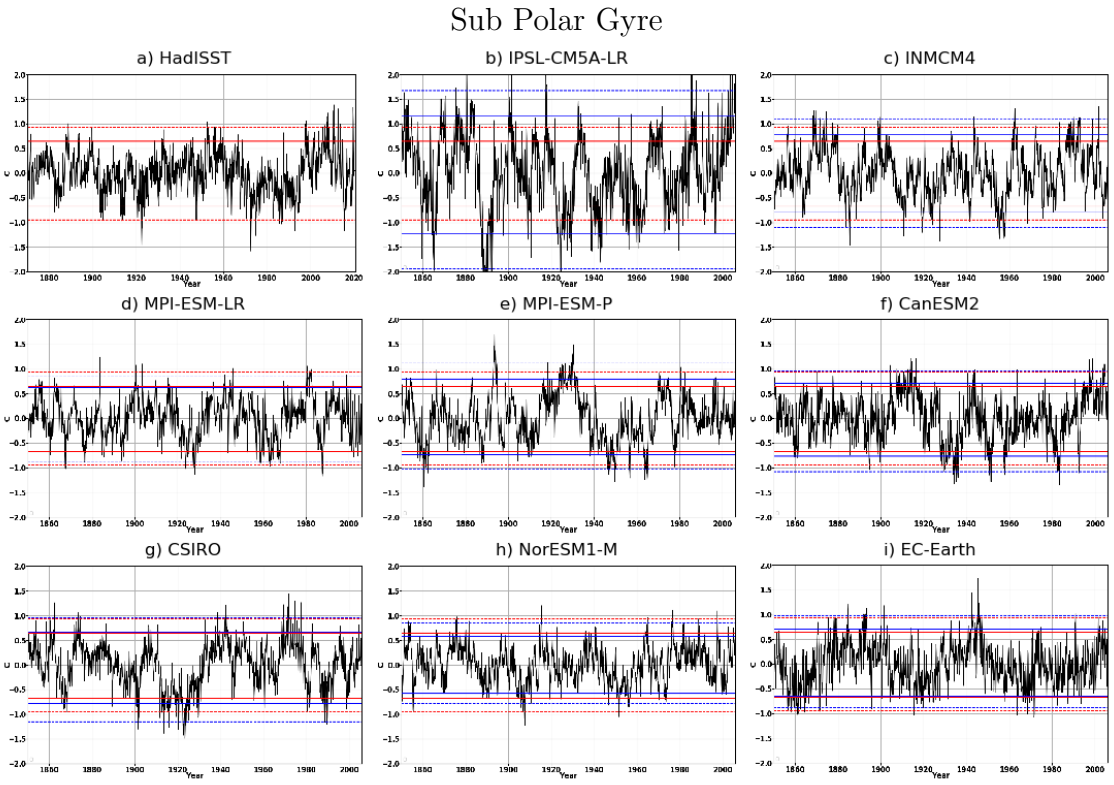

Figure 8: Red color lines represent the Observational data set 99th (- - -) percentile and 95th (——) percentile for ENSO region. The models 99th (- - -) and 95th (——) percentile for the ENSO region are represented by blue lines. The HadISST dataset spans from 1870 to 2020 whilst the models spans from 1850 to 2005.

Sub Polar Gyre								
Percentile	**EC-Earth**	**MPI-ESM-P**	**MPI-ESM-LR**	**CanESM2**	**CSIRO-MK3-6-0**	**INMCM4**	**IPSL-CM5A-L**	**NorESM1-M**
95th percentile	0.7	0.79	0.61	0.71	0.65	0.77	1.15	0.58
99th percentile	0.97	1.13	0.84	0.95	0.92	1.1	1.67	0.85
95 ratio	1.1	1.2	1.0	1.1	1.0	1.2	1.8	0.9
99 ratio	1.1	1.3	0.9	1.1	1.0	1.2	1.9	0.9

Table 6: Chart showing 95th and 99th percentiles performed by models. Percentile results were rounded to one decimal point. Ratios (red boxes) were created by dividing models results by corresponding percentile from HadISST. Pink shading highlights a similar representation of models to HadISST dataset results.

The Sub Polar Gyre region is accurately represented by CSIRO-MK3-6-0 model and similarly but underestimated by MPI-ESM-LR and overestimated by EC-Earth models. The rest of the models fail and overestimate by 1.6 on average. The model IPSL-CM5A-L almost doubles the overestimation of the temperature threshold value. Overall the Sub polar Gyre Region is a difficult area to estimate for most of the models but the CSIRO-MK3-6-0.

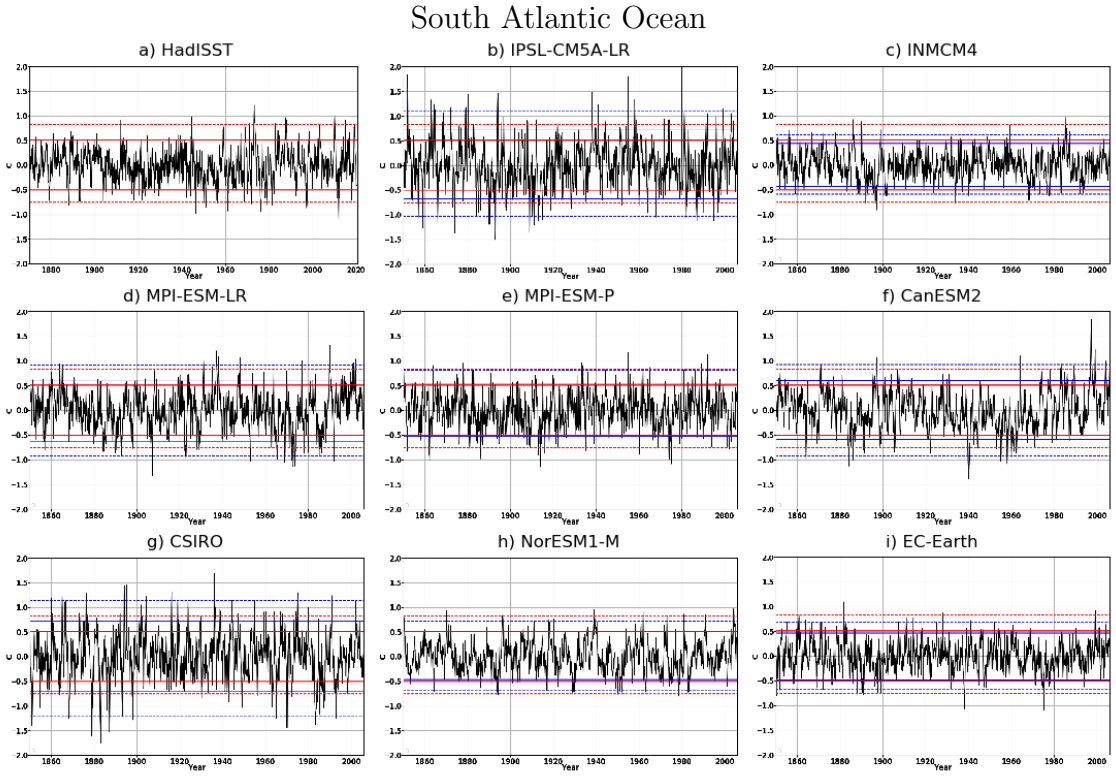

Figure 9: Red color lines represent HadISST dataset 99th (- - -) percentile and 95th (—) percentile for ENSO region. The models 99th (- - -) and 95th (—) percentile for the ENSO region are represented by blue lines. The HadISST dataset spans from 1870 to 2020 whilst the models spans from 1850 to 2005.

South Atlantic Region								
Percentile	**EC-Earth**	**MPI-ESM-P**	**MPI-ESM-LR**	**CanESM2**	**CSIRO-MK3-6-0**	**INMCM4**	**IPSL-CM5A-L**	**NorESM1-M**
95th percentile	0.46	0.53	0.58	0.6	0.71	0.43	0.71	0.51
99th percentile	0.68	0.8	0.91	0.92	1.13	0.61	1.1	0.72
95 ratio	0.92	1.0	1.16	1.2	1.42	0.86	1.42	1.0
99 ratio	0.8	1.0	1.1	1.1	1.4	0.7	1.3	0.9

Table 7: Chart showing 95th and 99th percentiles performed by models. Percentile results were rounded to one decimal point. Ratios (red boxes) were created by dividing models results by the corresponding percentile from HadISST. Pink shading highlights a similar representation of models to HadISST dataset results.

The South Atlantic Region displays a variety of results with some values close to precisely represent the threshold values. MPI-ESM-P model estimates the 99th percentile threshold value similar to HadISST results. CSIRO-MK3-6-0 is the model that fails the most on estimating the threshold value overestimating the threshold value with a 1.4 value. Overall, the South Atlantic Region proves to be difficult to estimate for most models being mostly overestimated.

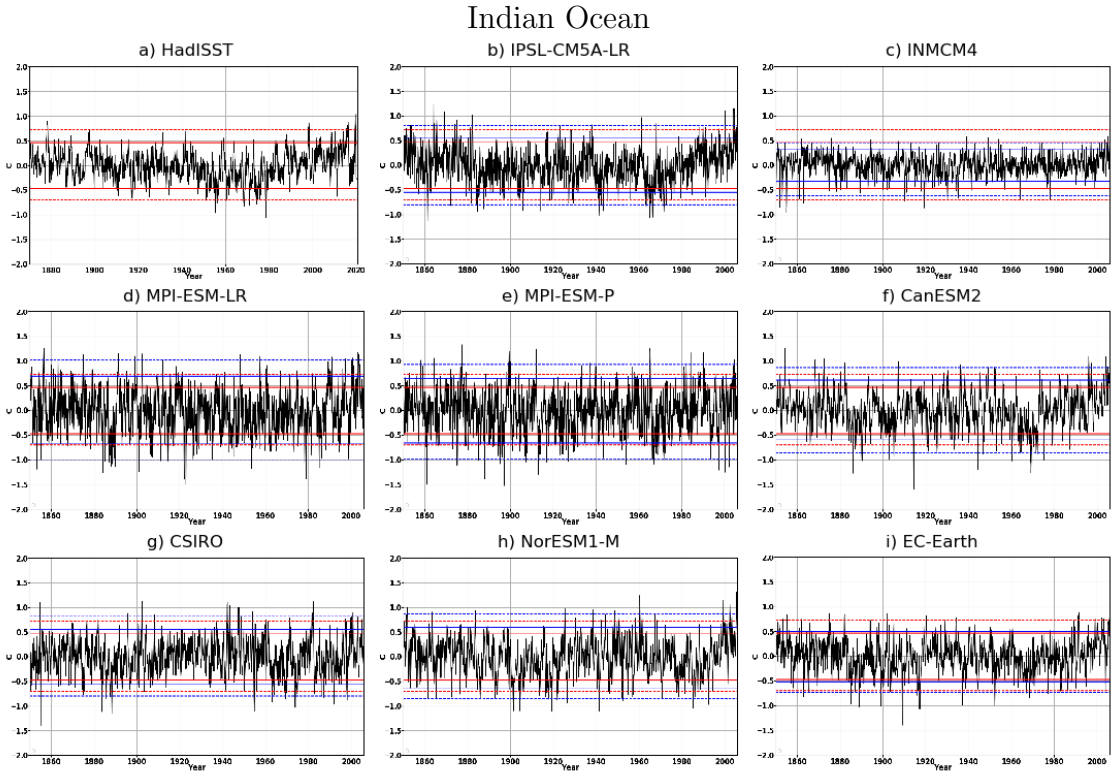

Figure 10: Red color lines represent tHadISST dataset 99th (- - -) percentile and 95th (——) percentile for ENSO region. The models 99th (- - -) and 95th (——) percentile for the ENSO region are represented by blue lines. HadISST dataset spans from 1870 to 2020, models time-frame spans from 1850 to 2005.

Indian Ocean Region								
Percentile	**EC-Earth**	**MPI-ESM-P**	**MPI-ESM-LR**	**CanESM2**	**CSIRO-MK3-6-0**	**INMCM4**	**IPSL-CM5A-L**	**NorESM1-M**
95th percentile	0.49	0.63	0.69	0.6	0.55	0.31	0.55	0.58
99th percentile	0.73	0.92	1.0	0.86	0.81	0.45	0.8	0.86
95 ratio	1.1	1.4	1.5	1.3	1.2	0.7	1.2	1.3
99 ratio	1.0	1.3	1.4	1.2	1.1	0.6	1.1	1.2

Table 8: Chart showing 95th and 99th percentiles performed by models. Percentile results were rounded to one decimal point. Ratios (red boxes) were created by dividing models results by corresponding percentile from HadISST. Pink shading highlights a similar representation of models to HadISST dataset.

The Indian Ocean region proves to be difficult for most of the models to precisely estimate the threshold values. Model EC-Earth is able to estimate the 99th percentile value precisely. All models agree with a warming at the end of the time series as well as the HadISST dataset, though HadISST show a warming starting around 1960's whilst models reflect a steady representation of SST's.

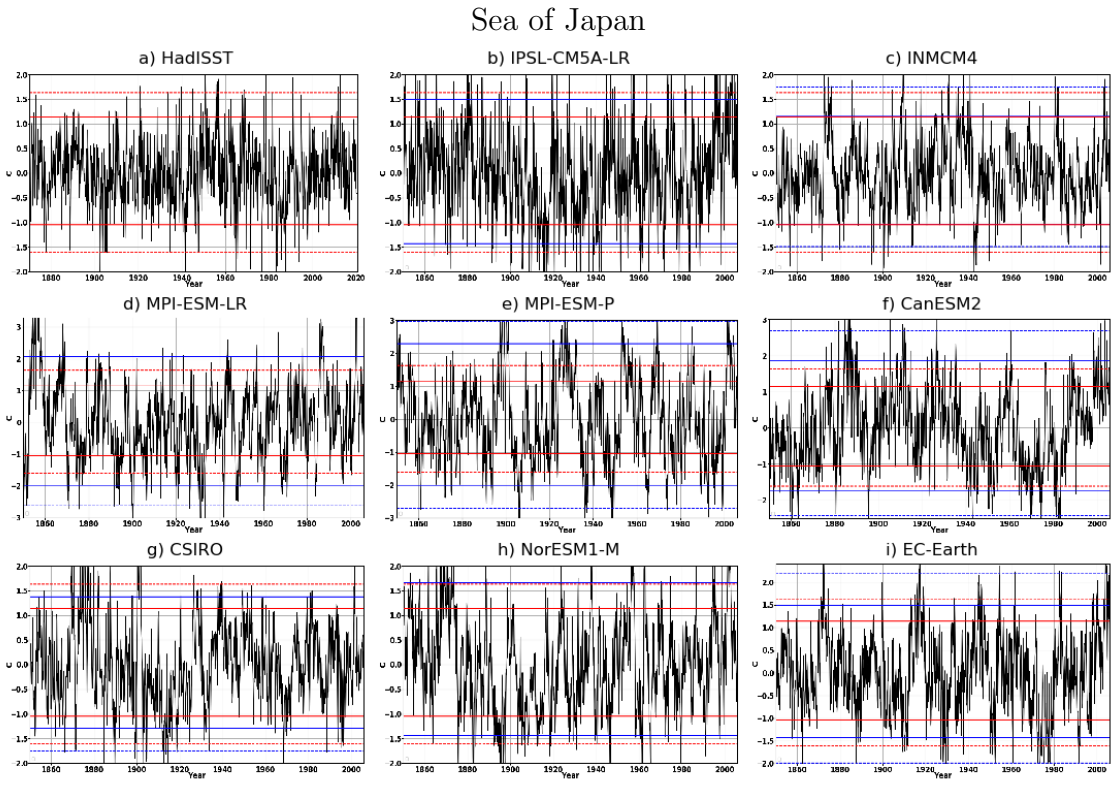

Figure 11: Red color lines represent the Observational data set 99th (- - -) percentile and 95th (——) percentile for ENSO region. The models 99th (- - -) and 95th (——) percentile for the ENSO region are represented by blue lines. HadISST dataset spans from 1870 to 2020 whilst the models spans from 1850 to 2005.

Sea of Japan								
Percentile	**EC-Earth**	**MPI-ESM-P**	**MPI-ESM-LR**	**CanESM2**	**CSIRO-MK3-6-0**	**INMCM4**	**IPSL-CM5A-L**	**NorESM1-M**
95th percentile	1.49	2.29	2.06	1.86	1.3	1.15	1.49	
99th percentile	1.3	1.8	2.0	1.6	1.3	1.1	1.3	1.4
95 ratio	1.3	2.0	1.8	1.6	1.1	1.0	1.3	1.5
99 ratio	1.3	1.8	2.0	1.6	1.3	1.1	1.3	1.4

Table 9: Chart showing 95th and 99th percentiles performed by models. Percentile results were rounded to one decimal point. Ratios (red boxes) were created by dividing models results by corresponding percentile from HadISST. Pink shading highlights a similar representation of models to HadISST results.

The Sea of Japan region is region with high variability, a region at which models overestimate the 99th percentile value. Two models nearly double their estimates over HadISST dataset. INMCM4 model represents the temperature values the closest to HadISST dataset, but still overestimating with a ratio of 1.1. Most models show a warming trend at the end of the time series whilst HadISST dataset shows neither warming or cooling.

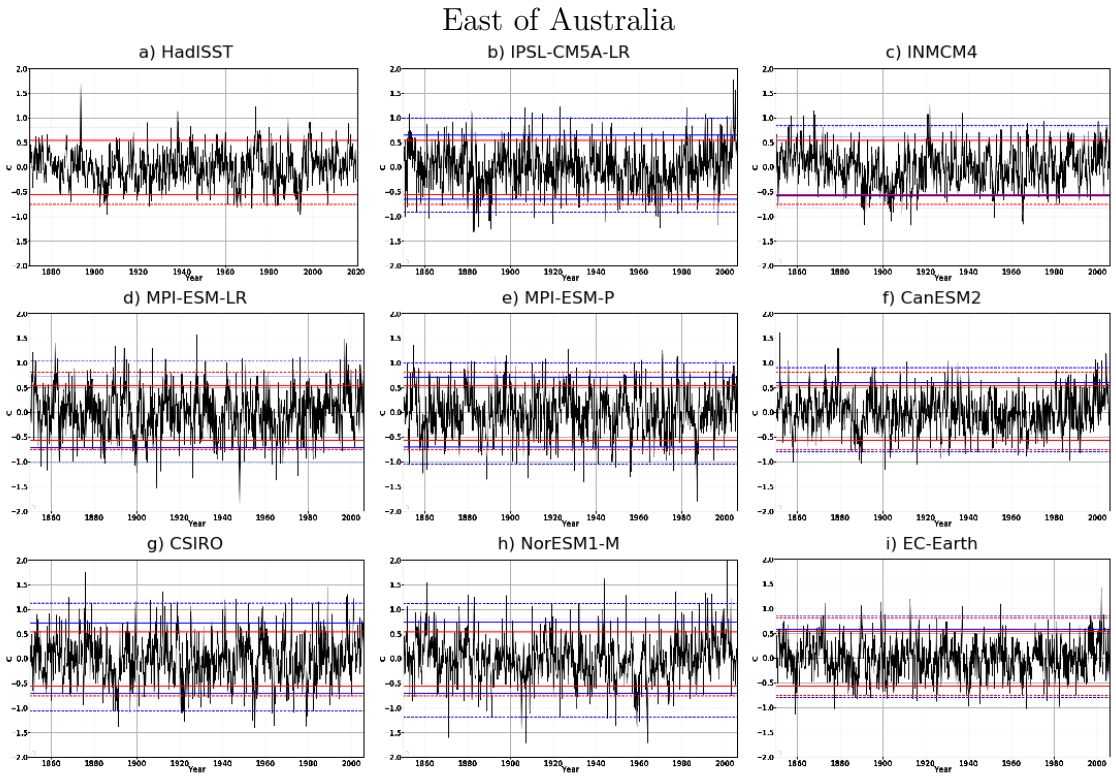

Figure 12: Red color lines represent the HadISST dataset 99th (- - -) percentile and 95th (——) percentile for ENSO region. The models 99th (- - -) and 95th (——) percentile for the ENSO region are represented by blue lines. The HadISST dataset spans from 1870 to 2020 whilst the models spans from 1850 to 2005.

Eastern Australia								
Percentile	**EC-Earth**	**MPI-ESM-P**	**MPI-ESM-LR**	**CanESM2**	**CSIRO-MK3-6-0**	**INMCM4**	**IPSL-CM5A-L**	**NorESM1-M**
95th percentile	0.57	0.71	0.73	0.59	0.72	0.6	0.64	0.73
99th percentile	0.84	1	1.03	1.12	0.83	0.98	1.12	
95 ratio	1.1	1.3	1.4	1.1	1.3	1.1	1.2	1.4
99 ratio	1.0	1.2	1.3	1.1	1.4	1.0	1.2	1.4

Table 10: Chart showing 95th and 99th percentiles performed by models. Percentile results were rounded to one decimal point. Ratios (red boxes) were created by dividing models results by corresponding percentile from HadISST. Pink shading highlights a similar representation of models to HadISST results.

The Eastern Australian region is precisely estimated by EC-Earth and INMCM4 models but overestimated by the rest of them. NorESM1-M and CSIRO-MK3-6-0 models overestimate the 99th percentile value with a 1.4 value. HadISST dataset does not show a clear trend of warming nor cooling. Whilst all models but NorESM1-M and CSIRO-MK3-6-0 get close HadISST SST's representation of the last decade.

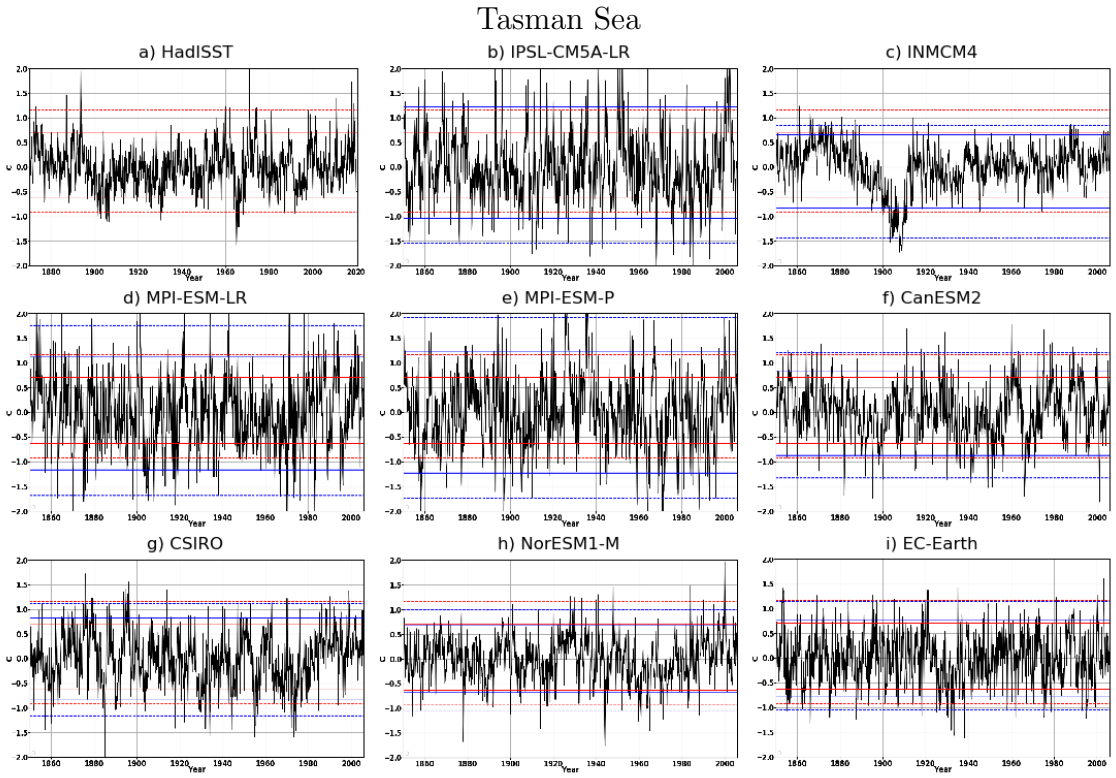

Figure 13: Red color lines represent the HadISST dataset 99th (- - -) percentile and 95th (—) percentile for ENSO region. The models 99th (- - -) and 95th (—) percentile for the ENSO region are represented by blue lines. The HadISST dataset spans from 1870 to 2020 whilst the models spans from 1850 to 2005.

Tasman Sea								
Percentile	**EC-Earth**	**MPI-ESM-P**	**MPI-ESM-LR**	**CanESM2**	**CSIRO-MK3-6-0**	**INMCM4**	**IPSL-CM5A-L**	**NorESM1-M**
95th percentile	0.77	1.23	1.12	0.83	0.82	0.65	1.22	0.67
99th percentile	1.14	1.91	1.75	1.2	1.12	0.84	2.0	1.0
95 ratio	1.1	1.8	1.6	1.2	1.2	0.9	1.7	1.0
99 ratio	1.0	1.6	1.5	1.0	1.0	0.7	1.7	0.9

Table 11: Chart showing 95th and 99th percentiles performed by models. Percentile results were rounded to one decimal point. Ratios (red boxes) were created by dividing models results by corresponding percentile from HadISST. Pink shading highlights a similar representation of models to HadISST dataset.

Tasman Sea region displays a similar behaviour to Eastern Australia's region. EC-Earth, CanESM2 and CSIRO-MK3-6-0 models estimate the threshold value similarly to HadISST. Models MPI-ESM-LR and MPI-ESM-P overestimate overestimated values over the 99th percentiles in respect to the HadISST dataset correspond to 1.5 and 1.6 respectively. Most models coincide with an increase on SST's at the end of the time series as noted at the HadISST dataset. A sudden drop in temperature can be seen at plot **c**, which may correspond to an error of the model at estimating temperature values at Tasman Sea region.

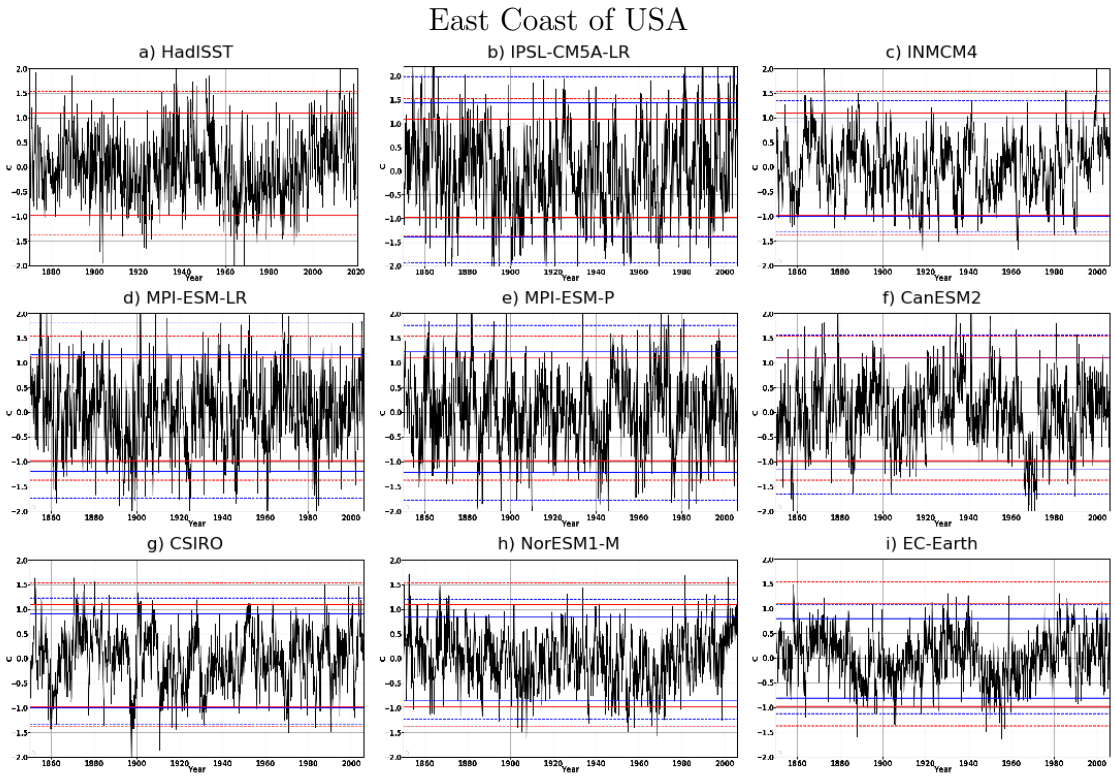

Figure 14: Red color lines represent the HadISST dataset 99th (- - -) percentile and 95th (——) percentile for ENSO region. The models 99th (- - -) and 95th (——) percentile for the ENSO region are represented by blue lines. HadISST dataset spans from 1870 to 2020 whilst the models spans from 1850 to 2005.

East Coast of USA								
Percentile	**EC-Earth**	**MPI-ESM-P**	**MPI-ESM-LR**	**CanESM2**	**CSIRO-MK3-6-0**	**INMCM4**	**IPSL-CM5A-L**	**NorESM1-M**
95th percentile	0.79	1.23	1.16	1.1	0.9	0.91	1.44	0.85
99th percentile	1.08	1.75	1.8	1.56	1.23	1.34	1.99	1.19
95 ratio	0.7	1.1	1.1	1.0	0.8	0.8	1.3	0.8
99 ratio	0.7	1.1	1.2	1.0	0.8	0.9	1.3	0.8

Table 12: Chart showing 95th and 99th percentiles performed by models. Percentile results were rounded to one decimal point. Ratios (red boxes) were created by dividing models results by corresponding percentile HadISST results. Pink shading highlights a similar representation of models to HadISST dataset.

The East Coast of the USA region is best estimated by model CanESM2. MPI-ESM-P and IPSL-CM5A-L models overestimate the 99th percentile value with a 1.2 and 1.3 values respectively. Most models agree with a warming trend at the end of the time-series around 2018. Models portray this region with high variability in agreement with HadISST results. Models INMCM4, NorESM1-M and EC-Earth have close representation of cycles and an upward warming trend presented in the last 10 years.

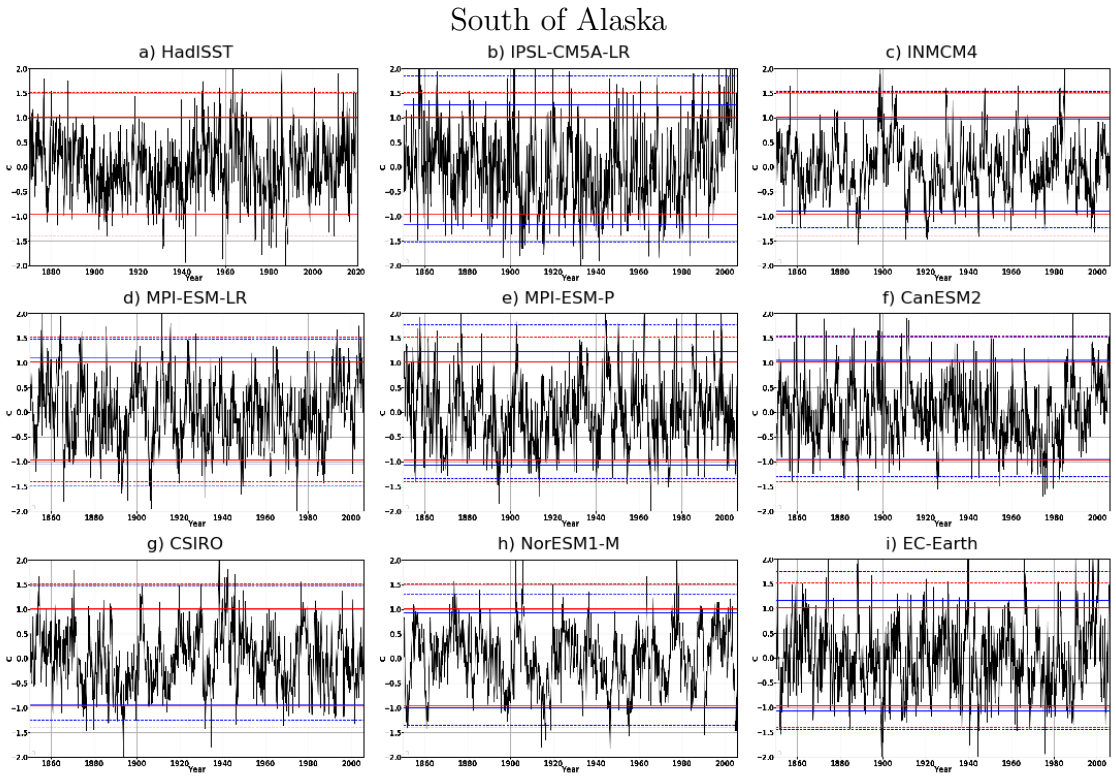

Figure 15: Red color lines represent the HadISST dataset 99th (- - -) percentile and 95th (——) percentile for ENSO region. The models 99th (- - -) and 95th (——) percentile for the ENSO region are represented by blue lines. HadISST dataset spans from 1870 to 2020 whilst the models spans from 1850 to 2005.

South of Alaska								
Percentile	**EC-Earth**	**MPI-ESM-P**	**MPI-ESM-LR**	**CanESM2**	**CSIRO-MK3-6-0**	**INMCM4**	**IPSL-CM5A-L**	**NorESM1-M**
95th percentile	1.16	1.23	1.09	1.05	1.01	0.96	1.26	0.93
99th percentile	1.74	1.76	1.48	1.53	1.46	1.54	1.84	1.3
95 ratio	1.1	1.2	1.1	1.0	1.0	1.0	1.2	0.9
99 ratio	1.2	1.2	1.0	1.0	1.0	1.0	1.2	0.9

Table 13: Chart showing 95th and 99th percentiles performed by models. Percentile results were rounded to one decimal point. Ratios (red boxes) were created by dividing models results by corresponding observations percentile. Pink shaded boxes indicate a similar representation of models at a particular region to HadISST dataset results.

MPI-ESM-LR, CanESM2, CSIRO-MK3-6-0 and INMCM4 represent the 99th percentile values similarly to HadISST 99th percentile values. Models EC-Earth, MPI-ESM-P and IPSL-CM5A-L overestimate the 99th threshold with a 1.2 value. Most models get close to a precise representation of the temperature threshold values meaning that the region is rather easy for those models to represent. IPSL-CM5A-LR, MPI-ESM-LR and CanESM2 present a similar upward warming trend at the end of the time series.

Models Performance								
Percentile	**EC-Earth**	**MPI-ESM-P**	**MPI-ESM-LR**	**CanESM2**	**CSIRO-MK3-6-0**	**INMCM4**	**IPSL-CM5A-L**	**NorESM1-M**
Accuracy	3	2	2	3	4	2	0	0
Area	Indian O.,Eastern Australia, Tasman Sea	ENSO, South Atlantic.	ENSO, South of Alaska	Tasman S., East Coast USA, South of Alaska	ENSO, SPG, Tasman S., South of Alaska	Eastern Australia, South of Alaska		

Table 14: Number of times and regions successfully estimated by models.

The number of precisely represented threshold values were counted to highlight the models skillful representation of SST's over 9 different regions. **CanESM2** model representation of threshold values are close to HadISST dataset for most regions, with a tendency to overestimate by 0.1 at Eastern Australian region as well as South Atlantic, Sub Polar Gyre. South of Japan and ENSO region are the most overestimated and underestimated regions with a 1.6 and 0.5 threshold values for the 99^{th} percentile respectively. On the other hand, its performance over Tasman sea, East coast of United States and South of Alaska are similar to the threshold values seen from HadISST dataset. **EC-Earth** model successfully represents the threshold values at the Indian Ocean Eastern Australian Region and Tasman Sea region and has good performance overall overestimating the Sub Polar Gyre and the South of Alaska regions with 1.1 and 1.2 respectively and underestimating the rest of the regions with the lowest value being 0.6 for the ENSO region. Overall EC-Earth model performs a similar distribution of SST's at South of Alaska and East Coast of the USA. The model that scores best among all models used in this study is **CSIRO-MK3-6-0**, representing four of the regions threshold values in a similar way to HadISST dataset. Overall, the model tends to overestimate threshold values with a maximum of 1.4 value for South Atlantic and Eastern Australian region. The only underestimated threshold value is done at the East coast of the United States with a 0.8 value.

Most models agree on displaying warming temperatures at the Northern hemisphere, mostly at coastal areas of Northern Canada, coast of Greenland, North of Europe and along Russia's Northern coast. Warming that might be affected by recent melting of the ice sheets. El Niño phenomenon is seen at all models but with different intensities and extension. Models INMCM4 and EC-Earth represent cooler temperatures than the rest of the models, perhaps showing La Niña phase of ENSO. Warming temperatures can be seen at the coast of Argentina near an area where the river *Rio de la Plata* outflows to the Atlantic Ocean. Perhaps this might be the cause for warm anomalies around that region as shown by models IPSL-CM5A-LR, INMCM4, MPI-ESM-LR and P, and NorESM1-M most notably.

5 Discussion and Conclusions

This study focuses on the sea surface temperature analysis to find the warmest temperatures experienced at different regions expressed by different models. The findings and implications of this study are presented and discussed at this section.

1. Climate models tend to overestimate temperature thresholds in most regions. Model resolution affects the representation of sea surface temperatures and varies amongst regions. Their ability to estimate influential climate modes like ENSO may be well represented in general but other influential processes like ocean currents tend to be overestimated or underestimated.

Differences amongst models can be rooted to their particular characteristics such as models resolution. A model working with a coarser resolution would display thermal differences at smaller regions of study with less detail than models with a finer resolution. Models NorESM1-ME, CanESM2, IPSL-CM5A-LR and INMCM4 have the highest resolution of the models used for this study. When comparing the performance of the models to represent the monthly temperature values over the 99^{th} percentile, the models with greater resolution display considerably less areas with values reaching up to ten months in a row over the threshold. Whilst observations mark large areas of warming over the 99^{th} percentile threshold at the equatorial Pacific, Caribbean Sea and Indian Ocean region. Models like MPI-ESM-LR and MPI-ESM-P with finer resolution (both with a 1.875° x 1.875° longitude latitude resolution) resemble the observation's temperature distribution and duration of temperatures mainly at Equatorial Pacific and Caribbean Sea in a similar way. Overall, the misrepresentation of duration and distribution of warming temperatures is more notable at models with a coarser resolution. Being most evident at the Atlantic and Indian Ocean regions where models show little similarities to observations.
Coarse resolution models IPSL-CM5A-LR, CanESM2 and NorESM1-M coincide in reflecting 1990's decade as the dominant warming decade, whereas MPI-ESM-LR and MPI-ESM-P with a finer resolution display a wide range of warming decades in smaller areas compared to coarser resolution models where larger areas tend to dominate. Coarser resolution models feature annual cycles difficult to remove from the time series even after creating the anomalies set and a detrending technique applied in a more consistent way that finer resolution models across different regions. The presence of annual cycles becomes more apparent the closer the region is to the poles. In the other hand, models at ENSO region show no presence of annual cycles due to its Equatorial location where the influence of annual cycles can be neglected. The internal variability of the models is also a factor that contributes to different outcomes amongst models despite of studying the same regions. The internal variability of models is described by the ensemble members which control the initial conditions used. All models in this study use the same parameterization and initialization states numbers but differ at the number of ensemble members. A general agreement on long-lasting warming trends around the Antarctic Ocean is reached by most models, though some models as well as observations show a warming at the coastal regions of Antarctica which can be a result of regional melting of sea ice. It is to note that most of the long-lasting warming months are close to coastal areas where river downstream or coastal processes influence temperature variance, such processes can be down-welling carrying cooler temperature to the surface.

2. Defining and monitoring marine heatwaves is heavily dependant on the configuration of the baseline period, the use of percentiles to assess the highest temperatures reached given the local context, and the model resolution used.

This study works with the 99^{th} percentile value as to filter extreme values from the entire time series. The use of a lower percentile would give us larger areas under constant warming and perhaps the inclusion of short and weak events that are not of interest for this study. Long time series are suitable for the use of the 99^{th} percentile because their appearance could tell us of sustained periods of time over the threshold value thru seasons that could result in ecological consequences. The use of a monthly time resolution highlights the areas under constant warming experienced over prolonged periods of time. The 99^{th} percentile ratio for the ENSO region shows that most models are able to mimic temperature thresholds limits similar to the observations with EC-Earth and CanESM2 models having the lowest ratio with a 0.6 and 0.5 respectively. On the other hand, the over estimation of the 99^{th} percentile by models in various regions makes it dangerous to confirm that marine heatwaves alone are the cause to the overestimated 99^{th} percentile limits. Such as the case of the IPSL-CM5A-L model that almost doubles the temperature thresholds by 2 at Sub polar Gyre and Tasman Sea regions. In combination with the use of the 99^{th} is the use of a fixed baseline covering the extension of the entire time series. The importance of choosing a fixed versus a moving baseline period is specifically related to the research question because it affects how the long-term trend in mean SST is expressed through MHW's. Using a contemporary baseline period is more suitable to studying ecosystems with rapid and greater mobility as this approach reflects shorter-term variability changes rather than long-term warming. The baseline period used for this study comprehends 150 years for HadISST dataset and 155 years for models, covering the entire time series. Which gives us a full analysis of long-term warming for our climatology compared to a fixed one.

3. Marine heatwaves formation owns its appearance to a number of factors including coastal processes, increase of greenhouse gases by human activities, teleconnection processes and western boundary currents.

Studying SST's gives us a hint about what could be happening in certain areas of interest. Accounting for involved processes into the formation of MHW's its necessary to conclude on their appearance. This study analyses SST's without accounting for any of the previously mentioned influential processes to differentiate what could be normal climate variance and the actual appearance of marine heatwaves over a defined threshold with its attached ecological consequences to marine wildlife. An alternative approach to study heatwaves and its potential impacts to marine wildlife could be based on choosing a threshold boundary derived from species tolerance to thermal changes.

4. High resolution models and the use of climate projections can provide greater detail around MHW's occurrence and effective adaptation planning around coastal areas.

Historical SST's studied over 1850 - 2005 in this research considered different metrics for assessment of MHW's appearance. Those metrics were sustained warming thru consecutive months, highest warming temperatures thru decades and warmest regions over the 99^{th} percentile. Results from consecutive warming displayed sustained warming periods highly influenced by climate modes and ocean processes (ENSO, Kuroshio/North Atlantic currents) in observations and most models. It is to note that the observational dataset show greater sustained warming at coastal regions, especially at the Pacific and Indian Ocean, but also around Antarctica and around Tasman sea and Eastern Australia. Overall CMIP5 models seem to solve coastal processes as there is little to white areas (wrong values) best seen at the Antarctic coast. The use of a finer resolution model for monthly assessment of MHW's could yield more realistic coastal phenomena where important marine resource exist. Together with a use of different Representative Carbon Pathways (RCP's) to project MHW's frequency, intensity and extension to better assessment of MHWs impacts and of adaptation plans. The use of a finer resolution gives a better detail of the spatial pattern of MHW's projected appearance influenced by western boundary currents [Hayashida, H. 2020], something that is difficult to do with models over 1° area as most CMPI5 models used in this study.

Warming over decades shows that most warming is experienced in recent decades, notably staring around 1980's and becoming more uniform at northern latitudes around 2010's decade as portrayed by observations. Most models agree with a recent warming staring at 1980's but fail to represent recent warming, that is because the observational data set spans up to the year 2020 whereas models only reach until 2005. HadISST dataset shows areas in white, which might be though to be warming experienced around 1870, but is rather the representation of missing values. Most models have areas in white color, where missing values appear, in some cases thru extended coastal areas as seen in model NorESM1-M at the Northwestern coast of Africa and around Japan as seen in model MPI-ESM-LR. According to models, highest warming experienced occurs at the Northern hemisphere around coastal areas of South of Greenland, Northern Europe and Russia as well as around Japan's coast. In contrast with observations, where highest warming is not visible at the Northern hemisphere but rather at the Antarctic coast, at ENSO region and to a smaller region off the East coast of Canada and United States. The explanation for this can be that models are sensitive to represent melting sea ice of the Arctic region and highly influenced by coastal processes like river run off, as seen at the coast of Argentina and the Sea of Japan where HadISST dataset results show weaker warming compared to most models. In conclusion, only a few models are able to represent recent or historical warming from 1870 to 2005 similar to the observational data set, which reduces the certainty over their estimations. Thus the use of finer resolution models and projections could reduce maladaptation plans aiming to reduce the impact of future MHW's.

5. Changes in temperature modulate species ability to survive. Mating and reproduction seasons as well as food resources and species migration are related to temperature ranges within species tolerance to thermal fluctuations.

SST's are the outcome of a combination of environmental factors such as wind stress, Up- and Down-welling, coastal processes and/or subsurface currents just to name a few. Thermal changes at any depth cause species to respond in a variety of ways. Species that can, will migrate to more suitable thermal environments with food source availability. The time at which thermal changes occur makes a difference on the possible outcomes to species survival. Progressive mean temperature changes occurring over prolonged periods of time gives species a chance to adapt, perhaps thru reducing their size or delaying their reproduction season to more suitable temperatures. Sudden and extreme temperature changes in the other hand, like a heatwave would be, could lead to acute heat deaths of species by pushing species thru their boundaries of tolerance. Availability of newer habitats for species and its interaction with their inhabitants is also a factor to species chances to survive. A negative interaction with new species could precipitate the collapse of its population by species competition or predation [Beaugrand, G.2015]. Findings from the HadISST dataset in this study show warm and sustained temperatures mostly at equatorial regions at Pacific, Atlantic and Indian Oceans. Being the ENSO region and coastal areas around the subindian continent where the largest areas of longest duration are found. Though most recent warming can be seen in the northern hemisphere, warming it is also notable in the southern hemisphere in recent decades indicating an overall warming of all regions of the world oceans, meaning an increase of MHW's of different duration and intensity. The highest warming seen at the observational dataset is found around Antarctica which can be explained by melting sea ice and the contrasts to extreme low temperatures found in the area. In contrast to HadISST dataset results, models show high levels of warming near coastal areas of the northern hemisphere whereas the southern hemisphere experiences smaller and lower intensity warming areas as portrayed by most models. The increasing warming experienced in the last decades shown by models and observations tell us that warming has become an increasing trend mostly in the northern hemisphere, thus we could not only expect marine heatwaves formation to increase but a heatwaves threshold value to be set in a recent basis. Increasing likelihood of marine heatwaves appearance can be expected and even a possible permanent MHW state can be reached if warming continues to rise, threatening not only species at sea but also human activities even far inland due to the potential increase of hurricanes formation and intensity due to higher energy stored at sea. Sea level rise due to thermal expansion of the oceans can trigger a set of threats to human populations living at coastal areas. Sea water intrusion can seriously damage the capacity of farmers to produce food this linked to food source availability at sea due to species migration. Sustained warming of the oceans experienced in the last decades combined with the effects of heatwaves of greater intensity and duration can marginally disrupt the way human populations have lived recently in the short term. Coral bleaching is sensitive to temperature, but is a time dependant exposure to temperature threshold limits what causes corals to bleach [Fitt W. et al 2001], like the one caused by sustained warming over temperature threshold limits caused by MHW's.

6. The use of climate models for impact assessment of MHW's on ecosystems must account for model skills and uncertainties at describing real world features. MHW's impact assessment can be better assessed by finer resolution model projections.

Findings of this study show differences between models to represent SST's threshold values of consecutive and decadal warming over the 99^{th} percentile as well as overall warming at different regions. Regions such as the South of Alaska are well estimated by most models but other areas selected in this study, like the Sea of Japan are overestimated by all models, some of which estimate the threshold values by two times the temperature values estimated by HadISST dataset. Which leads to think that there are not only regions that are difficult to estimate by models but the models in general that have a tendency to overestimate temperature values at certain regions compared to HadISST. **CSIRO-MK3-6-0** model outperforms all models estimations being able to represent threshold values similar to HadISST dataset in four occasions. In the other hand, **NorESM-M** model has the poorest performance of all, underestimating threshold values at most regions and only close to HadISST threshold values at ENSO region.

One of the reasons behind both models performance could be linked to its resolution. CSIRO-MK3-6-0 model presents a finer longitudinal resolution of 1.875° compared to a 2.5° longitudinal resolution from the NorESM-M model while the latitudinal resolution for both models are similar with a 1.875° and 1.894° respectively. Besides models resolution, another point of comparison could be their ensemble member from which the also differ. CSIRO-MK3-6-0 ensemble member is r10i1p1, its realization number is 10 which means its historical run starts long after the continuation of the spin-up run when the model output was considered to be more stable. Contrary to NorESM-M model where its ensemble member (r3i1p1) shows an earlier staring point after the control run has been made to mark the start of the 1850 historical run [Taylor, K. et al., 2012]. CMIP5 models resolution may be too coarse to solve mesoscale processes near coastal areas where important ecological systems are at stake [Hayashida H. et al,. 2020). A proposed alternative to a better assessment of MHW's impacts on marine wildlife near coastal areas could be the use of finer resolution model projections. For this matter projections running a low emission scenario (RCP 4.5) could be a good scenario to study MHW's future occurrence as this scenario is more in line with current emissions for a more realistic assessment of MHW's. CMIP5 models are too coarse resolution models to properly assess MHW's at coastal areas where important ecosystems are in danger, the use of models from CMIP5 program must be better used as a comparison to finer resolution models to understand CMIP5 models limits. When it comes to choose adaptation and mitigation measures or risk assessment studies, a better option to use would be RCP4.5 [Hausfather, Z.& G. Peters 2020]. The use of a more realistic scenario, compared to using RCP8.5 for instance, would help us avoid poor planning.

6 Acknowledgements

First of all, I would like recognize my supervisors Prof. Jens Hesselbjerg Christensen and Postdoc researcher Dominic Matte from the University of Copenhagen for their patience and supervision. Their invested time and shared skills were critical to the building of my knowledge about the climate. I would also like to thank family and friends whose support was invaluable to my performance as a student throughout my entire experience as a master degree student. I truly appreciate Niels Nymand assistance, whose guidance helped me develop an interest about the amazing world of programming. I would also like to express my appreciation to all the scientific community and modelling groups devoted to understand protect the environment.

A special thanks goes to CMIP5 program and the Hadley Centers Meteorological office for making available their Datasets.

7 References

– Beaugrand, G. (2015). Marine biodiversity, climatic variability and global change. Routledge.

– Borchert, L. F., Müller, W. A., & Baehr, J. (2018). Atlantic ocean heat transport influences interannual-to-decadal surface temperature predictability in the north atlantic region. Journal of Climate, 31(17), 6763-6782.

– Borchert, L. F., Pohlmann, H., Baehr, J., Neddermann, N. C., Suarez-Gutierrez, L., & Müller, W. A. (2019). Decadal predictions of the probability of occurrence for warm summer temperature extremes. Geophysical Research Letters, 46(23), 14042-14051.

– Collins M., M. Sutherland, L. Bouwer, S.-M. Cheong, T. Frolicher, H. Jacot Des Combes, M. Koll Roxy, I. Losada, K. McInnes, B. Ratter, E. Rivera-Arriaga, R.D. Susanto, D. Swingedouw, and L. Tibig, 2019: Extremes, Abrupt Changes and Managing Risk. In: IPCC Special Report on the Ocean and Cryosphere in a Changing Climate [H.-O. Portner, D.C. Roberts, V. Masson-Delmotte, P. Zhai, M. Tignor, E. Poloczanska, K. Mintenbeck, A. Alegria, M. Nicolai, A. Okem, J. Petzold, B. Rama, N.M. Weyer (eds.)]. In press.

– Data, C. (2009). Guidelines on analysis of extremes in a changing climate in support of informed decisions for adaptation. World Meteorological Organization.

– Dittus, A. J., Karoly, D. J., Donat, M. G., Lewis, S. C., & Alexander, L. V. (2018). Understanding the role of sea surface temperature-forcing for variability in global temperature and precipitation extremes. Weather and climate extremes, 21, 1-9.

– Fitt, W. K., Brown, B. E., Warner, M. E., & Dunne, R. P. (2001). Coral bleaching: interpretation of thermal tolerance limits and thermal thresholds in tropical corals. Coral reefs, 20(1), 51-65.

- Frölicher, T. L., & Laufkötter, C. (2018). Emerging risks from marine heat waves. Nature communications, 9(1), 650.
- Garrabou, J., Coma, R., Bensoussan, N., Bally, M., Chevaldonné, P., Cigliano, M., ... & Ledoux, J. B. (2009). Mass mortality in Northwestern Mediterranean rocky benthic communities: effects of the 2003 heat wave. Global change biology, 15(5), 1090-1103.
- Griffies, S. (2004). Fundamentals of ocean climate models. Princeton university press.
- Hibbard, K. A., G. A. Meehl, P. Cox, and P. Friedlingstein (2007): A strategy for climate change stabilization experiments. EOS, 88, 217, doi:10.1029/2007EO200002
- Hausfather, Z., & Peters, G. P. (2020). Emissions–the 'business as usual'story is misleading.
- Hayashida, H., Matear, R. J., Strutton, P. G., & Zhang, X. (2020). Insights into projected changes in marine heatwaves from a high-resolution ocean circulation model. Nature communications, 11(1), 1-9.
- Hobday, A. J., Alexander, L. V., Perkins, S. E., Smale, D. A., Straub, S. C., Oliver, E. C., ... & Holbrook, N. J. (2016). A hierarchical approach to defining marine heatwaves. Progress in Oceanography, 141, 227-238.
- Holbrook, N. J., Gupta, A. S., Oliver, E. C., Hobday, A. J., Benthuysen, J. A., Scannell, H. A., ... & Wernberg, T. (2020). Keeping pace with marine heatwaves. Nature Reviews Earth & Environment, 1-12.
- Hurrell, J. W., & Van Loon, H. (1997). Decadal variations in climate associated with the North Atlantic Oscillation. In Climatic change at high elevation sites (pp. 69-94). Springer, Dordrecht.
- Jacox, M. G., Alexander, M. A., Bograd, S. J., & Scott, J. D. (2020). Thermal displacement by marine heatwaves. Nature, 584(7819), 82-86.
- Kawale, J., Chatterjee, S., Kumar, A., Liess, S., Steinbach, M. S., & Kumar, V. (2011, October). Anomaly Construction in Climate Data: Issues and Challenges. In CIDU (pp. 189-203).
- Li, Z., Holbrook, N. J., Zhang, X., Oliver, E. C., & Cougnon, E. A. (2020). Remote forcing of Tasman Sea marine heatwaves. Journal of Climate, 33(12), 5337-5354.
- Loarie, S. R., Duffy, P. B., Hamilton, H., Asner, G. P., Field, C. B., & Ackerly, D. D. (2009). The velocity of climate change. Nature, 462(7276), 1052-1055.
- Mantua, N. J., & Hare, S. (2002). Pacific-Decadal Oscillation (PDO). Encyclopedia of global environmental change, 1, 592-594.
- Meehl, Gerald A., and Coauthors: Decadal Prediction. Bull. Amer. Meteor. Soc., 90, 1467–1485, doi:10.1175/2009BAMS2778.1, 2009.

- Meehl, G.A., and K.A. Hibbard, 2007: A strategy for climate change stabilization experiments with AOGCMs and ESMs. WCRP Informal Report No. 3/2007, ICPO Publication No. 112, IGBP Report No. 57, World Climate Research Programme: Geneva, 35 pp.
- Meehl, G. A., & Tebaldi, C. (2004). More intense, more frequent, and longer lasting heat waves in the 21st century. Science, 305(5686), 994-997.
- Mizuno, K., & White, W. B. (1983). Annual and interannual variability in the Kuroshio current system. Journal of physical oceanography, 13(10), 1847-1867.
- Mohan, S., & Bhaskaran, P. K. (2019). Evaluation and bias correction of global climate models in the CMIP5 over the Indian Ocean region. Environmental Monitoring and Assessment, 191(3), 806.
- Oliver, E. C., Benthuysen, J. A., Darmaraki, S., Donat, M. G., Hobday, A. J., Holbrook, N. J., ... & Gupta, A. S. (2021). Marine heatwaves.
- Oliver, E. C. (2019). Mean warming not variability drives marine heatwave trends. Climate Dynamics, 53(3), 1653-1659.
- Oliver, E. C., Burrows, M. T., Donat, M. G., Sen Gupta, A., Alexander, L. V., Perkins-Kirkpatrick, S. E., ... & Thomsen, M. S. (2019). Projected marine heatwaves in the 21st century and the potential for ecological impact. Frontiers in Marine Science, 6, 734.
- Ouzeau, G., Soubeyroux, J. M., Schneider, M., Vautard, R., & Planton, S. (2016). Heat waves analysis over France in present and future climate: Application of a new method on the EURO-CORDEX ensemble. Climate Services, 4, 1-12.
- Peterson, W., Robert, M., & Bond, N. (2015). The warm blob-Conditions in the northeastern Pacific Ocean. PICES Press, 23(1), 36.
- Rayner, N. A.; Parker, D. E.; Horton, E. B.; Folland, C. K.; Alexander, L. V.; Rowell, D. P.; Kent, E. C.; Kaplan, A. (2003) Global analyses of sea surface temperature, sea ice, and night marine air temperature since the late nineteenth century J. Geophys. Res.Vol. 108, No. D14, 4407 10.1029/2002JD002670
- Reverdin, G. (2010). North Atlantic subpolar gyre surface variability (1895–2009). Journal of climate, 23(17), 4571-4584.
- Reynolds, R. W. (1988). A real-time global sea surface temperature analysis. Journal of climate, 1(1), 75-87.
- Scannell, H. A., Pershing, A. J., Alexander, M. A., Thomas, A. C., & Mills, K. E. (2016). Frequency of marine heatwaves in the North Atlantic and North Pacific since 1950. Geophysical Research Letters, 43(5), 2069-2076.
- Simmons, A. J., Berrisford, P., Dee, D. P., Hersbach, H., Hirahara, S., & Thépaut, J. N. (2017). A reassessment of temperature variations and trends from global reanalyses and monthly surface climatological datasets. Quarterly Journal of the Royal Meteorological Society, 143(702), 101-119.

- Taylor, K. E., Stouffer, R. J., & Meehl, G. A. (2012). An overview of CMIP5 and the experiment design. Bulletin of the American Meteorological Society, 93(4), 485-498.

- Thompson, D. W., Wallace, J. M., Jones, P. D., & Kennedy, J. J. (2009). Identifying signatures of natural climate variability in time series of global-mean surface temperature: Methodology and insights. Journal of Climate, 22(22), 6120-6141.

- Wang, G., & Schimel, D. (2003). Climate change, climate modes, and climate impacts. Annual Review of Environment and Resources, 28(1), 1-28.

- World Meteorological Organization. (2017). WMO guidelines on the calculation of climate normals.

- Wu, L., Cai, W., Zhang, L., Nakamura, H., Timmermann, A., Joyce, T., ... & Giese, B. (2012). Enhanced warming over the global subtropical western boundary currents. Nature Climate Change, 2(3), 161-166.

- Wu, Z., Huang, N. E., Long, S. R., & Peng, C. K. (2007). On the trend, detrending, and variability of nonlinear and nonstationary time series. Proceedings of the National Academy of Sciences, 104(38), 14889-14894.

- Zhang, J., & Zhang, R. (2015). On the evolution of Atlantic meridional overturning circulation fingerprint and implications for decadal predictability in the North Atlantic. Geophysical Research Letters, 42(13), 5419-5426.

8 Appendix

In order to obtain detrended anomalies from data sets a series of techniques are applied to the various data sets. Firstly, the influence of annual cycles must be removed. This is done by subtracting the reference period (150 years) monthly mean to the corresponding month. For example,subtracting all Januaries mean from the entire climate series from every January included in the time series. The procedure repeats for the following months throughout the time-series. Then a detrending method is applied to have a better lecture of our data and finally the 99^{th} threshold value is marked into our detrended data set. The following plots will show how the data plots change as every step to process our data is applied in for the HadISST data set.

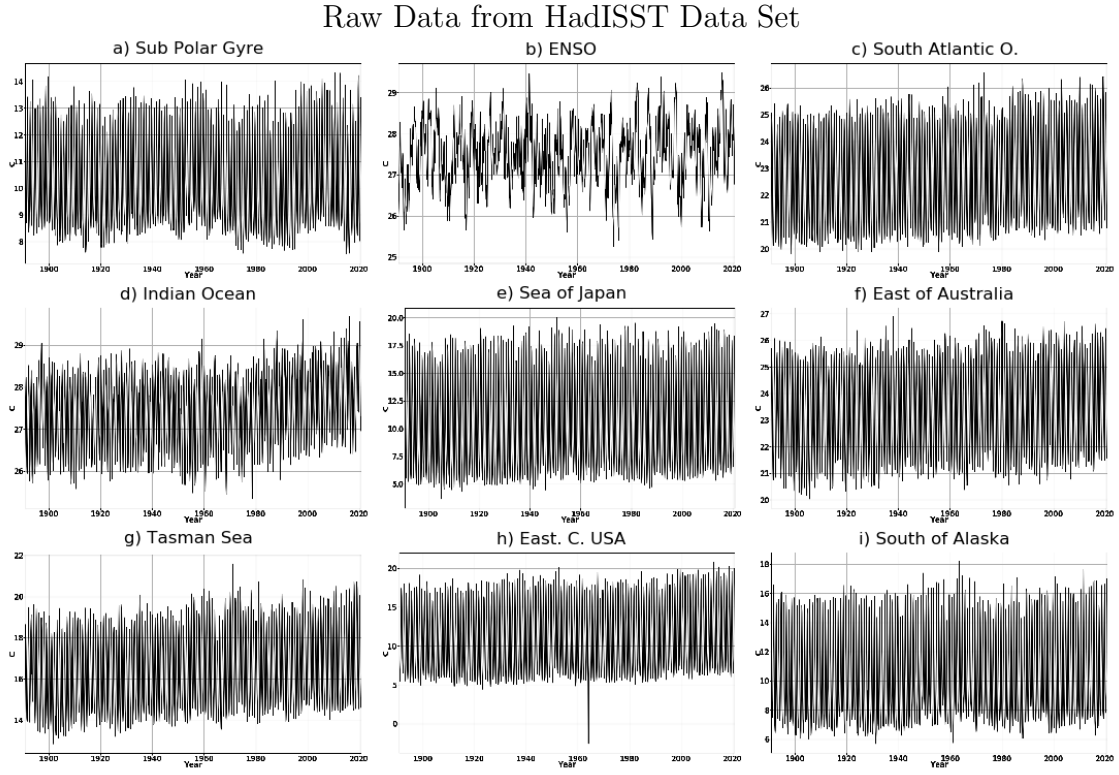

Figure 16: Annual cycles influence and trend is seen over all regions but ENSO. The geographical location of ENSO limits the influence of annual cycles displaying a rather "clean" SST's variance throughout the time-series. The observational dataset spans from 1870 to 2020. Plot h) shows an abrupt low temperature value which can be considered an error value from the observational dataset.

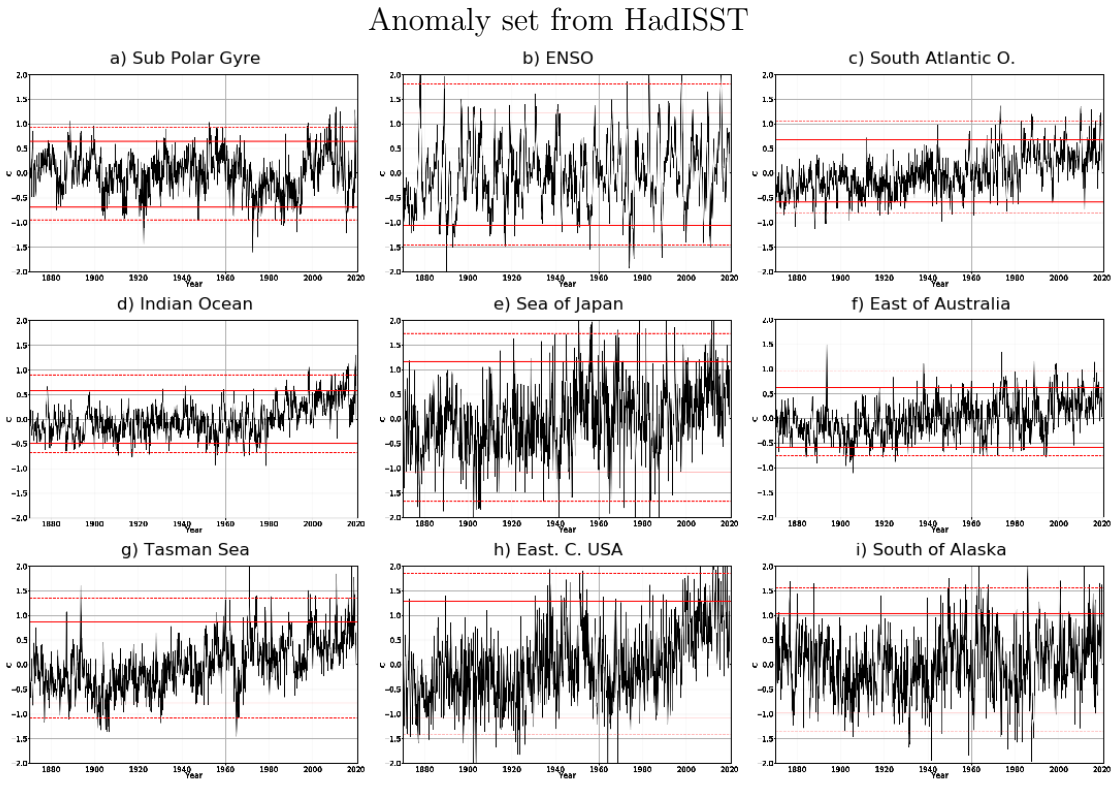

(a) Shows plots with annual cycles influence removed and 1^{st}(- - -), 5^{th}(——), 95^{th}(——) and 99^{th}(- - -) percentiles. The anomaly set considers a time period spanning thru the length of the time-series, 150 years.

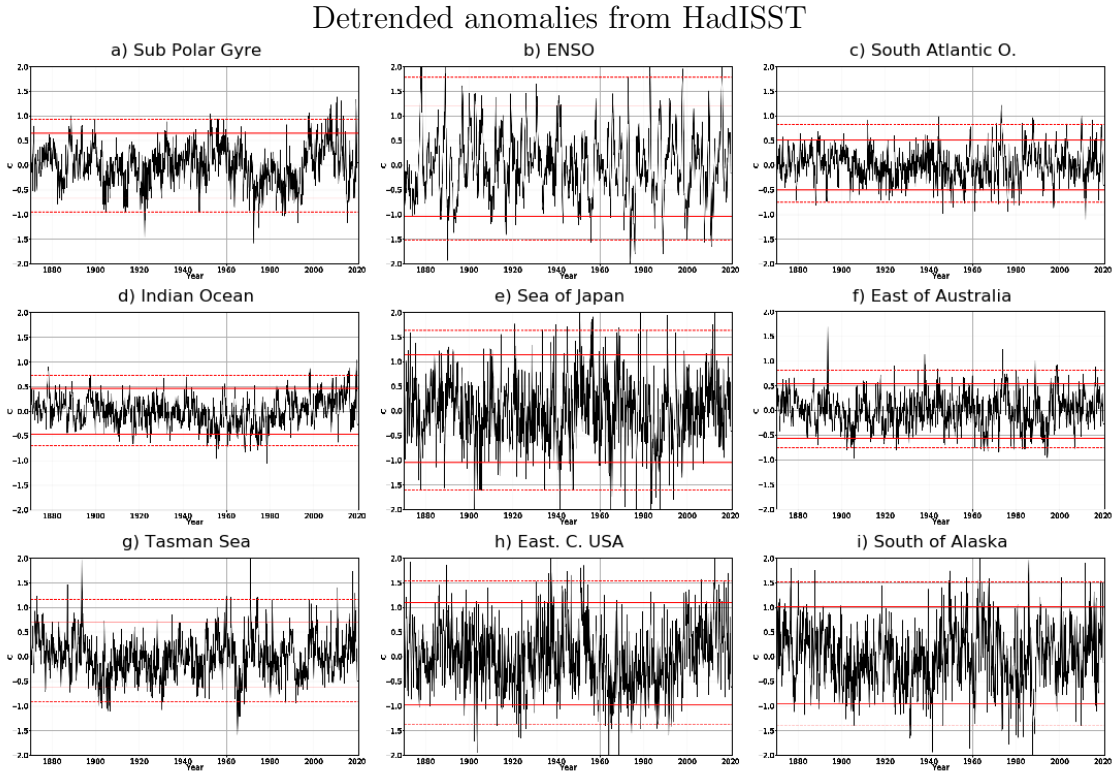

Figure 18: Detrended SST's anomaly values of HadISST observational dataset are shown in this figure. 1^{st}(- - -), 5^{th}(——), 95^{th}(——) and 99^{th}(- - -) percentiles.

Some models are able to remove the seasonal cycles in a more efficient way than others. To put this into perspective two different models will be showing the how they perform throughout the process. EC-Earth model and NorESM1-M will be shown for this purpose. EC-Earth models proved to have a good performance in most regions and was best ranked amongst all models whilst NorESM1-M has an average overestimation of 2 times the observational data set temperatures threshold.

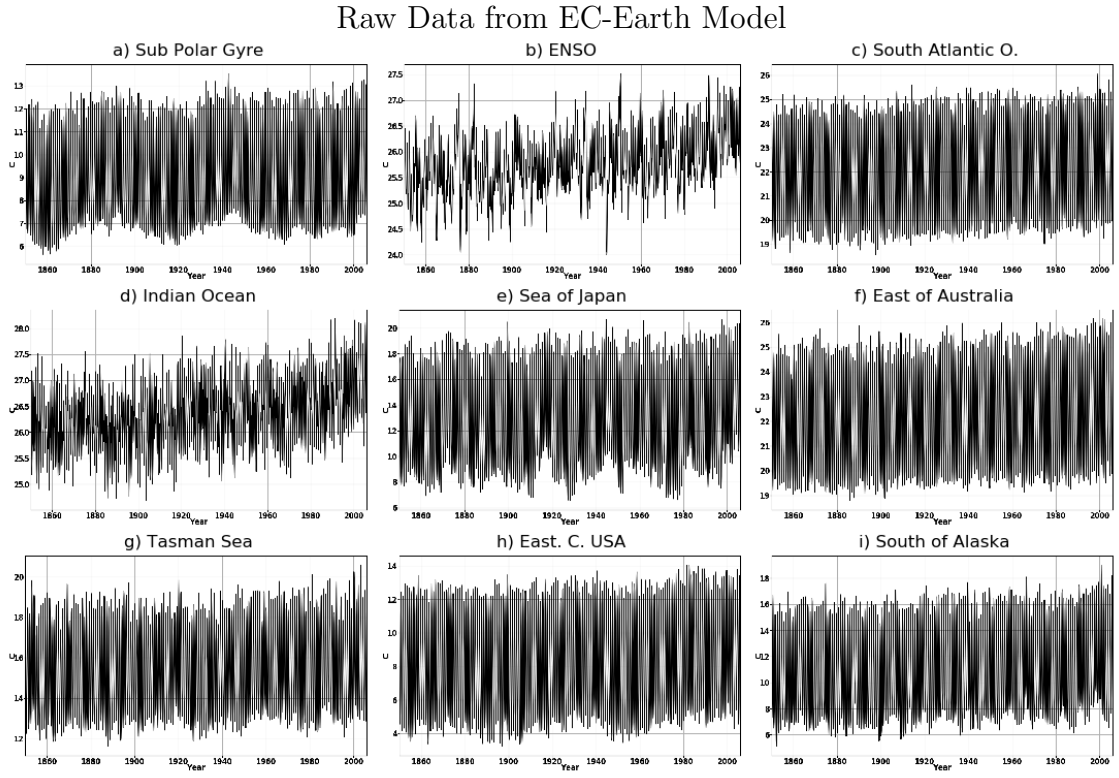

Figure 19: Annual cycles and trend are easily identifiable at all locations but ENSO, a feature seen at all models. Time-series of models span from 1850 to 2005.

Figure 20: Anomaly set from EC-Earth

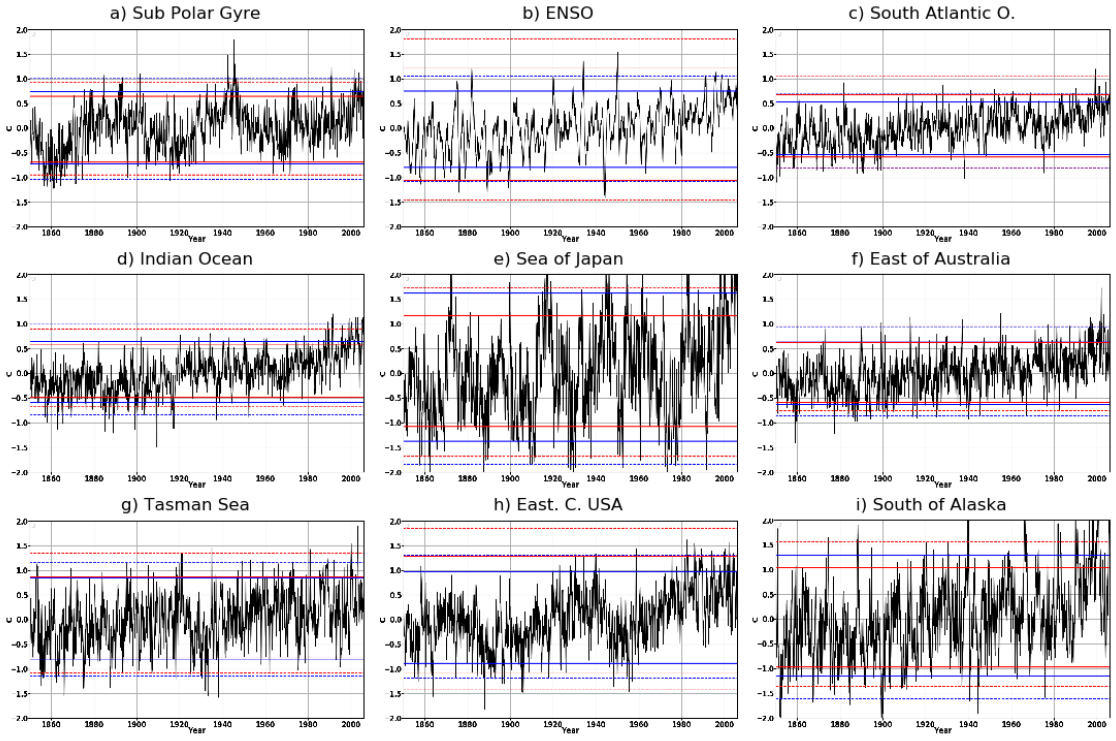

Figure 21: Shows plots 1^{st}(- - -), 5^{th}(——), 95^{th}(——) and 99^{th}(- - -) percentiles. The anomaly set considers a time period spanning from 1850 to 2005.

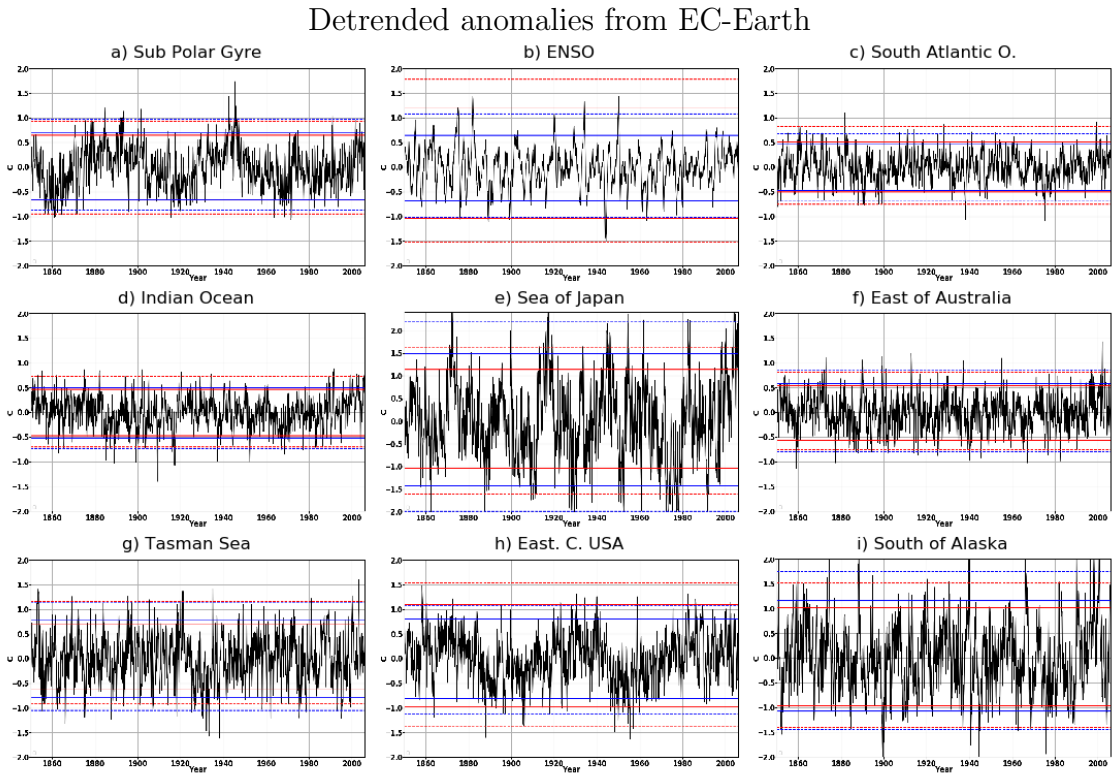

Figure 22: Detrended SST's anomaly values of EC-Earth model are shown in this figure. 1^{st}(- - -), 5^{th}(——), 95^{th}(——) and 99^{th}(- - -) percentiles.